# ORIGINAL RESEARCH

Coordinated Cross-Talk Between the Myc and Mlx Networks in Liver Regeneration and Neoplasia

Huabo Wang,[1] Jie Lu,[1] Frances Alencastro,[2,3] Alexander Roberts,[1] Julia Fiedor,[1] Patrick Carroll,[4] Robert N. Eisenman,[4] Sarangarajan Ranganathan,[5] Michael Torbenson,[6] Andrew W. Duncan,[2,3,7] and Edward V. Prochownik[1,7,8,9]

[1]Division of Hematology/Oncology, Children's Hospital of Pittsburgh, University of Pittsburgh Medical Center, Pittsburgh, Pennsylvania; [2]Department of Pathology, University of Pittsburgh Medical Center, Pittsburgh, Pennsylvania; [3]McGowan Institute for Regenerative Medicine, University of Pittsburgh Medical Center, Pittsburgh, Pennsylvania; [4]Basic Sciences Division, Fred Hutchinson Cancer Research Center, Seattle, Washington; [5]Department of Pathology, Cincinnati Children's Hospital, Cincinnati, Ohio; [6]Department of Laboratory Medicine and Pathology, The Mayo Clinic, Rochester, Minnesota; [7]Pittsburgh Liver Research Center, University of Pittsburgh, Pittsburgh, Pennsylvania; [8]Hillman Comprehensive Cancer Center, University of Pittsburgh Medical Center, Pittsburgh, Pennsylvania; and [9]Department of Microbiology and Molecular Genetics, University of Pittsburgh Medical Center, Pittsburgh, Pennsylvania
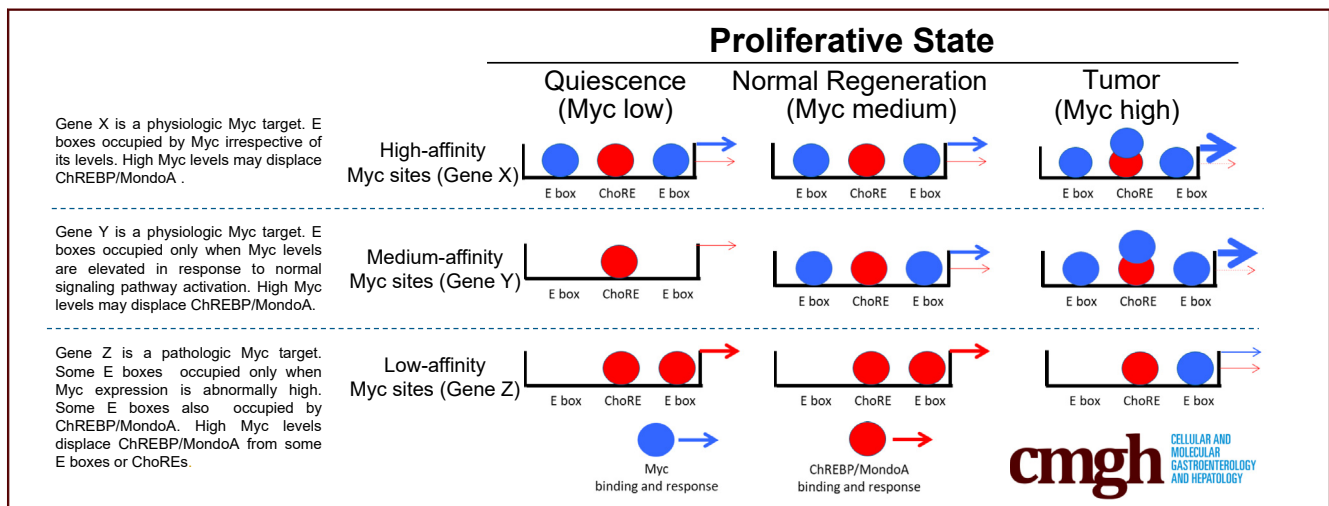
SUMMARY

The Myc and Mlx Networks show extensive crosstalk and regulate distinct but overlapping sets of transcriptional targets. The current work shows the cooperation between these 2 networks in supporting the regenerative capabilities of normal hepatocytes while also showing that the Mlx Network serves as a suppressor of spontaneous hepatic adenomatosis.

BACKGROUND & AIMS: The c-Myc (Myc) Basic helix-loop-helix leucine zipper (bHLH-ZIP) transcription factor is deregulated in most cancers. In association with Max, Myc controls target genes that supervise metabolism, ribosome biogenesis, translation, and proliferation. This Myc network crosstalks with the Mlx network, which consists of the Myc-like proteins MondoA and ChREBP, and Max-like Mlx. Together, this extended Myc network regulates both common and distinct gene targets. Here, we studied the consequence of *Myc* and/or *Mlx* ablation in the liver, particularly those pertaining to hepatocyte proliferation, metabolism, and spontaneous tumorigenesis.

METHODS: We examined the ability of hepatocytes lacking *Mlx* (*Mlx*KO) or *Myc+Mlx* (double KO [DKO]) to repopulate the liver over an extended period of time in a murine model of type I tyrosinemia. We also compared this and other relevant behaviors, phenotypes, and transcriptomes of the livers with those from previously characterized *Myc*KO, *Chrebp*KO, and *Myc*KO × *Chrebp*KO mice.

RESULTS: Hepatocyte regenerative potential deteriorated as the Extended Myc Network was progressively dismantled. Genes and pathways dysregulated in *Mlx*KO and DKO hepatocytes included those pertaining to translation, mitochondrial function, and hepatic steatosis resembling nonalcoholic fatty liver disease. The Myc and Mlx Networks were shown to crosstalk, with the latter playing a disproportionate role in target gene regulation. All cohorts also developed steatosis and molecular evidence of early steatohepatitis. Finally, *Mlx*KO and DKO mice showed extensive hepatic adenomatosis.

CONCLUSIONS: In addition to showing cooperation between the Myc and Mlx Networks, this study showed the latter to be more important in maintaining proliferative, metabolic, and translational homeostasis, while concurrently serving as a

suppressor of benign tumorigenesis. GEO accession numbers: GSE181371, GSE130178, and GSE114634. *(Cell Mol Gastroenterol Hepatol 2022;13:1785–1804; https://doi.org/10.1016/j.jcmgh.2022.02.018)*

C-Myc (Myc) is a Basic helix-loop-helix leucine zipper (bHLH-Zip) transcription factor that regulates numerous target genes, which collectively support survival, proliferation, metabolism, ribosome biogenesis and translation.[1–8] Positive regulation involves Myc's direct sequence-specific DNA binding in heterodimeric association with its obligate bHLH-Zip partner, Max.[6,7] This occurs at canonical E-box elements that typically reside in the vicinity of proximal promoters.[9–12] Bound Myc–Max heterodimers recruit an assortment of transcription co-factors and chromatin modifiers such as histone acetylases and methyltransferases, which collectively increase chromatin accessibility, relieve transcriptional pausing, and increase the rate and efficiency of messenger RNA (mRNA) elongation.[13–17] Down-regulation of these genes, often occurring during cellular quiescence or differentiation, involves a reduction in Myc levels and a shift in E-box occupancy to heterodimers now comprising Max and members of the transcriptionally repressive bHLH-ZIP Mxd family, which includes Mxd1–4 and the less-related Mnt and Mga factors.[3,18–20] Together, their binding reverses the chromatin modifications mediated by Myc–Max binding and restores transcriptional repression. Negative regulation by Myc is more indirect and involves interaction with and inhibition of positively acting transcription factors such as Miz1 and Sp1.[21,22] The loss of transcriptional balance maintained by these different competing interactions is a feature of transformed cells, which often overexpress and/or otherwise deregulate Myc.[4,10,14,23]

The Myc Network crosstalks and shares considerable regulatory overlap with a structurally related but distinct group of bHLH-Zip transcription factors that comprise the so-called Mlx Network.[1–3,8,20,24,25] Classically believed to control target gene sets smaller and more functionally restricted than those overseen by Myc, the Myc-like equivalents of the Mlx Network include the transcription factors Carbohydrate response element (ChRE)-binding protein (ChREBP) and MondoA. Upon binding glucose and other nutrients, these cytoplasmic proteins translocate to the nucleus, heterodimerize with the Max-like protein Mlx, and bind to their target genes at carbohydrate response elements (ChoREs) comprising tandem E-boxes separated by 5 nucleotides.[26,27] Myc Network and Mlx Network members (collectively termed the *Extended Myc Network*) can bind to one another's DNA target sequences and some genes are dually regulated by both sets of factors; however, the numbers of these genes and the degree to which their regulation is a result of binding to shared vs separate sites has not been delineated clearly.[28–32] Although the Mlx Network is less widely implicated in tumorigenesis than the Myc Network, recurrent *MLX* gene deletions nevertheless occur in as many as 10%–20% of several human cancers, with the precise fraction correlating with the size of the deletion (https://portal.gdc.cancer.gov/genes/ENSG00000108788).[1–3,13,20,33]

We previously explored the roles for these 2 networks in normal hepatocyte proliferation using mice lacking the enzyme fumarylacetoacetate hydrolase (FAH). These animals serve as a model for type I hereditary tyrosinemia in which FAH's absence allows toxic tyrosine catabolites to accumulate, leading to hepatic necrosis and liver failure.[34–36] Treatment with the drug 2-[2-nitro-4-trifluoromethylbenzoyl]-1,3-cyclohexanedione (NTBC) blocks the enzyme 4-hydroxyphenylpyruvic dioxygenase, which catalyzes the second step in tyrosine catabolism, thereby preventing the accumulation of these deleterious intermediates and circumventing the lethal consequences of FAH deficiency. Immunocompromised fumarylacetoacetate hydrolase nonobese diabetic (FRG-NOD) ($Fah^{-/-}$) mice thus can be used as a robust and sensitive animal model in which to evaluate the regenerative potential of any other hepatocyte population, so long as it is $Fah+/+$. Cells are delivered intrasplenically followed by the cyclic withdrawal and reinstatement of NTBC over several months. As recipient hepatocytes accumulate toxic tyrosine intermediates and die, they are replaced by the donor cells, which expand as much as 50- to 100-fold before eventually comprising up to 70% of the hepatic mass and allowing the recipients to achieve NTBC independence.[25,37] The FAH model thus places greater proliferative demands on regenerating hepatocytes than does two-thirds partial hepatectomy (PH), which represents the gold standard for liver regeneration.[38] It also permits the simultaneous delivery of 2 or more competing populations of hepatocytes to the same recipient, thus allowing for a direct comparison of their relative proliferative rates within the identical environment.

Using this approach, we previously showed that wild-type (WT) and *Myc-/-* (*Myc*KO) hepatocytes possess indistinguishable regenerative potential.[37] This is quite different from most other cases in which Myc's loss in either nontransformed or transformed cells or tissues profoundly suppresses proliferation.[25,37,39–43] In contrast, the

proliferation of *Chrebp-/-* (*Chrebp*KO) hepatocytes is impaired significantly and *Myc*KO × *Chrebp*KO hepatocytes are even more defective.[25] These findings indicated that normal hepatocyte regeneration is more dependent on the Mlx Network than the Myc Network and that the 2 pathways crosstalk and rescue one another's defects to varying degrees. At the same time, they raise questions about the possible functional redundancy of MondoA in the context of ChREBP's loss.

We now have explored the relationship between the Myc and Mlx Networks further by generating 2 additional mouse strains. In the first (hereafter referred to as *Mlx*KO), deletion of the *Mlx* gene functionally inactivates the entire Mlx Network, including any potential rescue by MondoA that might have existed in *Chrebp*KO mice.[25] The second mouse strain contains a double knockout (DKO) of both *Myc* and *Mlx* that further inactivates the Extended Myc Network. We show that hepatocytes from both strains, but particularly the latter, are profoundly compromised in repopulating the livers of *Fah-/-* recipients. They also show markedly attenuated expression of genes that are direct targets for both the Myc and Mlx Networks and that control mitochondrial structure and function, ribosomal biogenesis, and more general aspects of mRNA processing and translation. Older mice of both groups also develop steatosis akin to that previously described in *Myc*KO, *Chrebp*KO, or *Myc*KO × *Chrebp*KO mice. Finally, and unexpectedly, more than one third of older *Mlx*KO and DKO mice develop multifocal hepatic adenomas occasionally associated with small regions of hepatocellular carcinoma (HCC). These results further support the idea that the Myc and Mlx Networks crosstalk and cooperatively regulate a range of pathways related to energy metabolism, lipid balance, translation, and proliferation. Finally, they show a heretofore unsuspected role for the Mlx Network as a suppressor of benign hepatic adenomatosis.[44]

Results

Repopulation by MlxKO and DKO Hepatocytes Is Severely Compromised

Donor mouse strains used for competitive hepatocyte repopulation studies carried homozygous floxed alleles of the *Mlx* and/or *Myc* genes (Figure 1*A* and *B* and Table 1) and expressed an albumin promoter–driven tamoxifen-inducible estrogen receptor and Cre recombinase (CreER).[25,45] Five daily intraperitoneal injections of tamoxifen were sufficient to allow inactivation of each allele by the time hepatocytes were transplanted 3–4 months later (Figure 1*C*).

Using FRG-NOD mice as recipients, we previously showed that WT donor hepatocytes can outcompete an equal number of *Chrebp*KO hepatocytes whereas WT and *Myc*KO hepatocytes compete equally.[25,35,37] Suspecting that *Mlx*KO hepatocytes would be even more defective, and to emphasize this, we delivered a total of 3×10^5 donor hepatocytes intrasplenically into recipient mice at an approximately 1:6 WT:*Mlx*KO ratio (Figure 2*A* and *B*). After 24–28 weeks of NTBC cycling, a number of recipients had died and no survivors had achieved NTBC independence, possibly as

a result of the deliberate under-representation of WT hepatocytes in the initial inoculum. Indeed, quantification of the total donor population in the surviving recipients indicated that it comprised only 2%–46% of all hepatocytes, which is both lower and more variable than typically achieved when mice receive larger numbers of replication-competent donor cells (Figure 2*C*).[25,37] Despite this low-level reconstitution, the surviving donor hepatocytes were nearly all WT despite their initial minority status (*P* < .001) (Figure 2*D*).

Although *Myc* deletion alone does not confer a replicative disadvantage to hepatocytes, *Chrebp* deletion does and is exacerbated further by the concurrent inactivation of *Myc*.[25] This suggests that the Myc and Mlx Networks are redundant and compensate for one another under certain circumstances. Because *Myc*KO × *Chrebp*KO hepatocytes still express MondoA,[25] we asked whether its redundancy might mask more prominent phenotypes. We therefore compared the replicative potential of a mixed population of WT and DKO hepatocytes (1:10 ratio) in which the latter cells have functionally inactivated both ChREBP and MondoA as a consequence of *Mlx* deletion. This experiment achieved a somewhat greater rate of transplant success, with more animals surviving and with recipient livers eventually containing more than 50% donor hepatocytes (Figure 2*E*). As before, however, virtually all of these were of WT origin (*P* < .001) (Figure 2*F*).

To determine more directly which KO population was more proliferatively challenged, an additional competitive transplant experiment was performed using a 1:1 input ratio of *Mlx*KO and DKO donor hepatocytes. Overall survival again was low, no animals achieved NTBC independence and less than 2% of hepatocytes isolated from recipients were of donor origin (Figure 2*G*). However, despite their own inherent replicative compromise, *Mlx*KO hepatocytes showed an overwhelming survival advantage (Figure 2*H*) and comprised nearly 95% of the recovered donor population (*P* < .001). Together, these results argue that, in a highly demanding, long-term model of liver regeneration,[25,37,46,47] *Mlx* loss and the ensuing functional inactivation of ChREBP and MondoA markedly compromise donor hepatocyte proliferation and/or survival, with the additional loss of *Myc* strongly reinforcing the defect.

Overlapping Transcriptional Dysregulation in MlxKO and DKO Livers Primarily Involves Genes With Roles in Mitochondrial Structure and Function and Translation

Before comparing whole-transcriptome profiles of WT, *Mlx*KO, and DKO livers, we confirmed that the latter 2 evidenced the predicted dysregulation of their direct target genes. For this, gene set enrichment analysis[48] was performed on 3 collections of direct Myc target genes from the Molecular Signatures Data Base C2 collection (MSigDB) (http://www.gsea-msigdb.org/gsea/msigdb/collections.jsp) and a 154-member panel of MondoA/ChREBP/Mlx direct target genes from the Qiagen Ingenuity Pathway Analysis (IPA) data set (Table 2). In the first case, 2 of the 3 Myc
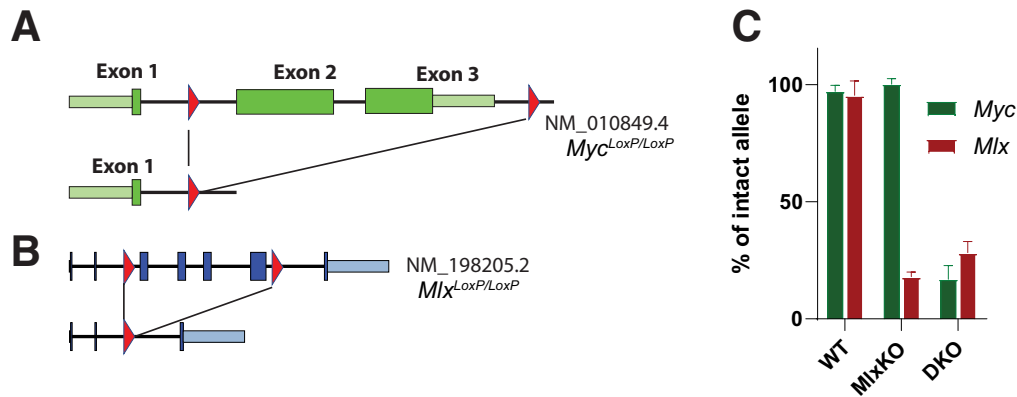
Figure 1. Strategies for the quantification of total donor and recipient hepatocytes and donor subpopulations.
(*A*) Relevant regions of the murine *Myc* locus before and after CreER-mediated recombination showing the location of LoxP sites flanking coding exons 2 and 3 (*red triangles*).[25,37] (*B*) Relevant regions of the *Mlx* locus before and after CreER-mediated recombination showing the location of LoxP sites flanking coding exons 3 and 6.[8] (*C*) Verification of *MlxKO* and DKO. (*A–C*) Four to 5 weeks after CreER activation, DNA from the indicated livers was assessed for the presence of intact or recombined *Myc* and *Mlx* alleles. Hepatocytes then were used for transplant studies. Low levels of nonexcised genes likely originated from the nonhepatocyte populations present in the liver.[25,37]

Table 1. Quantitative Polymerase Chain Reaction Primers and Probes Used to Quantify Each Allele Shown in Figure 1*A* and *B* and Other Necessary Genes as Indicated

| Name	Sequence of primers and probes	GenBank accession number	Location	Target
Fah-/-	Forward: 5'-GGGAGGATTGGGAAGACAATAG-3' Reverse: 5'-ATTCTCCTTGCCTCTGAACATAA-3' Probe: 5'/56-FAM/CTTCTGAGG/ZEN/ CGGAAAGAACCAGCT/3IABkFQ/3'	KF947529 NM_010176 KF947529	4896-4917 657-635 4950-4973	bGH_PA_terminator FAH bGH_PA_terminator
GFP	Forward: 5'-AGTGCTTCAGCCGCTACC-3' Reverse: 5'-GAAGATGGTGCGCTCCTG-3' Probe: 5'/56-FAM/TTCAAGTCC/ZEN/GCCA TGCCCGAA/3IABkFQ/-3'	MT776902 MT776902 MT776902	302-319 393-376 346-366	eGFP eGFP eGFP
Mlx WT	Forward: 5'-TAGCCCAGTGAAGGTCTCA-3' Reverse: 5'-AGGAGTAGACAGGGTAGCTAAT-3' Probe: 5'/56-FAM/CAGGTCCAG/ZEN/ CTTTAGCCCATGTCA/3IABkFQ/3'	NC_000077.7 NC_000077.7 NC_000077.7	100980807- 100980825 100980911- 100980890 100980856- 100980879	Mlx Mlx Mlx
Mlx-/- (MlxKO)	Forward: 5'-CACAGGTAGGCAGCAACATA-3' Reverse: 5'-GGAGTGAGGGTGTCTTGTAATC-3' Probe:5' /56-FAM/CGCCCTTCT/ZEN/ ACCCTGTCTACTCCT/3IABkFQ/3'	NC_000077.7 NC_000077.7 N/A	100979147- 100979166 100980990- 100980969 N/A	Mlx Mlx Loxp site
Myc WT	Forward: 5'-GGGAATCCTCACATTCCTACTT-3' Reverse: 5'-GATTCAGCACTGGGTGCA-3' Probe: 5'/56-FAM/TAGGAAGAC/ZEN/ TGCGGTGAGTCGTGA/3IABkFQ/3'	NC_000081.7 NC_000081.7 NC_000081.7	61858492- 61858513 61858643- 61858626 61858549- 61858572	Myc Myc Myc
Myc-/- (MycKO)	Forward: 5'-TGATCTGAGCGGTTCCGTA-3' Reverse: 5'-TAAAGTCCCAAAGACACTCCAG-3' Probe: 5'/56-FAM/CCTGCACGA/ZEN/ TCCGGAACCCTTAAT/3IABkFQ/3'	NC_000081.7 NC_000081.7 NC_000081.7	61858570- 61858588 61863536- 61863515 61858624- 61858629	Myc Myc Myc+ loxp site
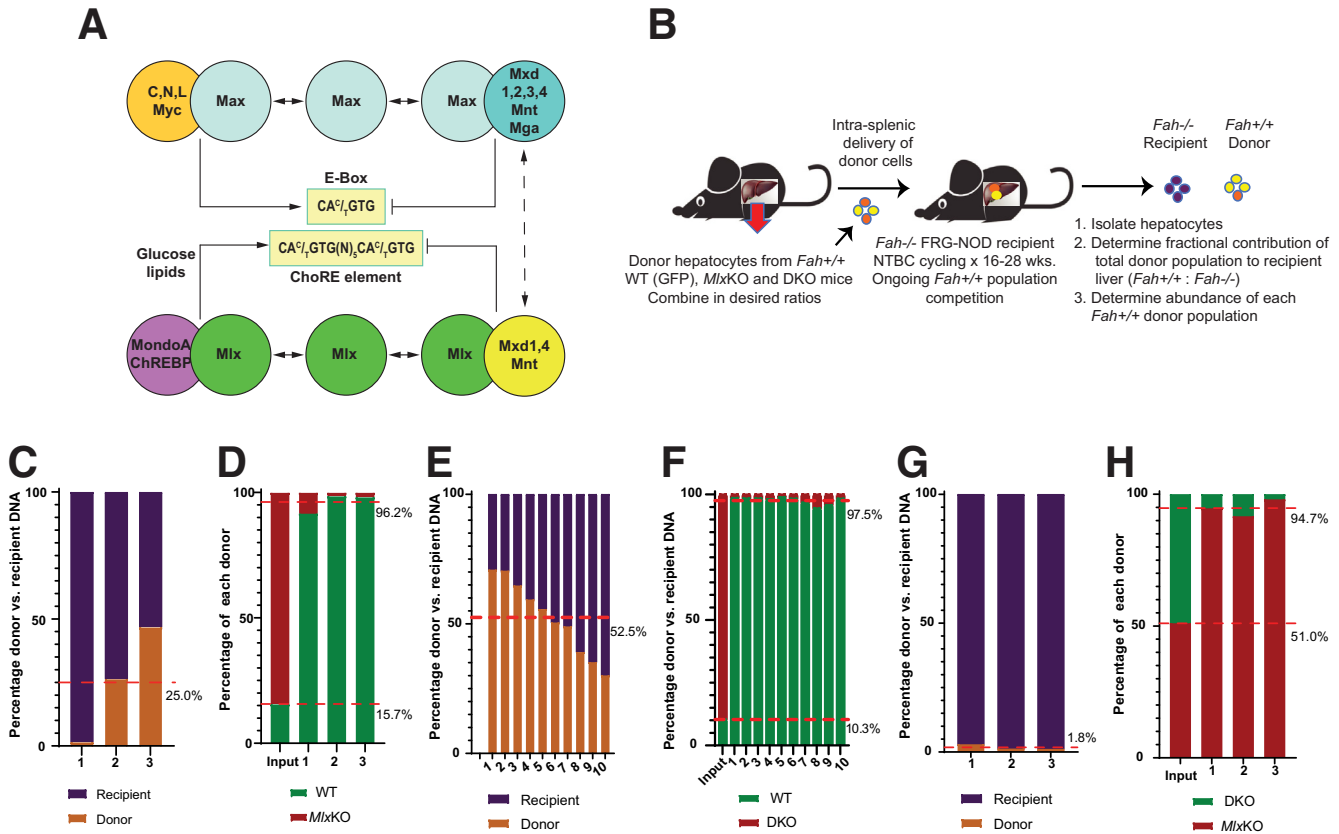
Figure 2. WT hepatocytes outcompete *Mlx*KO and DKO hepatocytes in repopulation assays. (*A*) The extended Myc Network. *Top*: Myc Network, comprising Myc, Max, Mxd1–4, Mnt, and Mga1 and their consensus E-box binding site. *Bottom*: Mlx Network and its E-box–related but more complex ChoRE binding site.[27,46] Mlx interacts with the nutrient-regulated positive factors ChREBP and MondoA or the negative factors Mxd1, Mxd4, and Mnt.[2,13,24] The latter cross-talk with the Myc Network (*dotted arrow*). (*B*) Hepatocyte transplantation strategy. Isolated *Fah*+/+ WT or KO hepatocytes were mixed at the desired ratio and injected intrasplenically into FRG-NOD *Fah*$^{-/-}$ mice maintained continuously on NTBC. NTBC cycling was continued until mice achieved NTBC independence or for 24–28 weeks, at which time total hepatocytes were isolated and the fractional representation of the total donor and recipient populations was determined (Figure 1). The contribution of each donor set then was further determined and compared with that of the input inoculum. (*C*) After intrasplenic injection of 3×10^5 donor hepatocytes comprising a 1:6 ratio of WT and *Mlx*KO cells, NTBC cycling was continued for 24–28 weeks in the 3 animals that survived, with none achieving NTBC independence. Hepatocyte DNA was isolated from the transplanted animals and the percentage of recipient and total donor cells was determined. (*D*) DNA from panel *C* was used to determine the ratio of the WT and *Mlx*KO donor populations. DNA from an aliquot of hepatocytes at the time of transplant was used to confirm the input donor cell ratio. (*E*) Transplants performed in FRG-NOD *Fah*$^{-/-}$ mice using inocula containing an approximate 1:10 ratio of WT:DKO cells. Hepatocytes isolated after 24–28 weeks of NTBC cycling showed that, on average, 52.5% of hepatocytes were composed of donor cells. (*F*) Hepatocyte DNA from panel *E* was used to determine the fraction of WT and *Mlx*KO donor hepatocytes. *Lane 1* shows the approximate 1:10 ratio of the initial input inoculum. (*G*) Transplants performed in FRG-NOD *Fah*$^{-/-}$ mice using inocula containing an approximate 1:1 ratio of *Mlx*KO and DKO cells. Total hepatocytes isolated after 24–28 weeks of NTBC cycling were evaluated for the fractional representation of total donor and recipient populations showing that, on average, less than 2% of the total hepatocyte mass was of donor origin. (*H*) Fractional make-up of the donor population from panel *G*. *Lane 1* shows the approximate 1:1 ratio of the input population.

target gene sets also were enriched significantly in *Mlx*KO liver RNA sequencing profiles, indicating as previously shown that some Myc-regulated genes also are responsive to Mlx Network inactivation (Figure 3*A*).[13,24,25] The broader and more pronounced enrichment of these transcripts in DKO livers indicated that the Myc Network further contributes to the Mlx Network–mediated regulation of these targets as expected. In the second case, MondoA/ChREBP/Mlx target genes were enriched significantly in both *Mlx*KO and DKO livers (Figure 3*B*). These results confirmed that

Myc and/or *Mlx* inactivation was associated with both unique and shared responses of each network's respective target genes.

To assess the effect of progressive dismantling of the extended Myc Network on target gene sets, volcano plots were used to compare individual gene expression profiles in the earlier-described livers and previously described *Myc*KO, *Chrebp*KO, and *Myc*KO × *Chrebp*KO livers (GEO accession number: GSE114634).[25] In the latter 3 cases, fewer than 30 differences were identified relative to normal livers from age-

Table 2. MondoA, ChREBP, and Mlx Direct Target Genes From the Qiagen IPA Data Set

Symbol	Entrez gene ID	Symbol	Entrez gene ID	Symbol	Entrez gene ID	Symbol	Entrez gene ID
Acaca	107476	Mrc1	17533	Rpl30	19946	Rps2	16898
Acacb	100705	Mtor	56717	Rpl31	114641	Rps20	67427
Acly	104112	Nr0b1	11614	Rpl32	19951	Rps21	66481
Acss2	60525	Nr1d1	217166	Rpl35	66489	Rps23	66475
Adgre1	13733	Pck1	18534	Rpl35a	57808	Rps24	20088
Adipor2	68465	Pgd	110208	Rpl36	54217	Rps25	75617
Agps	228061	Pklr	18770	Rpl36a	19982	Rps26	27370
Anxa2	12306	Plin1	103968	Rpl36al	66483	Rps27	57294
Arntl	11865	Pnpla2	66853	Rpl37	67281	Rps27rt	100043813
Ccl2	20296	Pnpla3	116939	Rpl37a	19981	Rps27a	78294
Ccl7	20306	Ppara	19013	Rpl38	67671	Rps27l	67941
Ccn3	18133	Pparg	19016	Rpl39	67248	Rps28	54127
Cebpa	12606	Ppargc1a	19017	Rpl39l	68172	Rps29	20090
Cidec	14311	Pygl	110095	Rpl3l	66211	Rps3	27050
Cpt1a	12894	Rgs16	19734	Rpl4	67891	Rps3a1	20091
Dhrs7b	216820	Rpl10	110954	Rpl41	67945	Rps4y1	20102
Elovl6	170439	Rpl10a	19896	Rpl5	100503670	Rps5	20103
Fabp4	11770	Rpl11	67025	Rpl6	19988	Rps6	20104
Fasn	14104	Rpl12	269261	Rpl6l	432502	Rps7	20115
Fgf21	56636	Rpl13	270106	Rpl7	19989	Rps8	20116
Foxa1	15375	Rpl13a	22121	Rpl7a	27176	Rps9	76846
Foxa2	15376	Rpl14	67115	Rpl7l1	66229	Rpsa	16785
G6pc	14377	Rpl15	66480	Rpl8	26961	Scap	235623
Gnpat	14712	Rpl17	319195	Rpl9	20005	Scd	20249
Gpam	14732	Rpl18	19899	Rplp0	11837	Sirt1	93759
Gpat3	231510	Rpl18a	76808	Rplp1	56040	Slc2a2	20526
Gpd1	14555	Rpl19	19921	Rplp2	67186	Slc2a4	20528
Hmgcr	15357	Rpl21	19933	Rps10	67097	Srebf1	20787
Hnf1a	21405	Rpl22	19934	Rps11	27207	Srsf2	20382
Hnf4a	15378	Rpl22l1	68028	Rps12	20042	Thbs2	21826
Igf2	16002	Rpl23	65019	Rps13	68052	Thrb	21834
Il1rn	16181	Rpl23a	268449	Rps14	20044	Thrsp	21835
Itgax	16411	Rpl24	68193	Rps15	20054	Tkfc	225913
Khk	16548	Rpl26	19941	Rps15a	267019	Tkt	21881
Lgals3bp	19039	Rpl27	19942	Rps16	20055	Txnip	56338
Lipe	16890	Rpl27a	26451	Rps17	20068	Ucp1	22227
Mlx	21428	Rpl28	19943	Rps18	20084	Ucp3	22229
Mlxip	208104	Rpl29	19944	Rps19	20085		
Mlxipl	58805	Rpl3	27367	Rps19bp1	66538		

matched animals (differential expression, ≥1.5-fold and q < 0.05), whereas *Mlx*KO and DKO livers showed up to 60-fold more differences (Figure 3*C*). This more pronounced gene dysregulation again suggested that the combined loss of ChREBP and MondoA eliminated all redundant functions from the Mlx Network, thereby allowing a much larger complement of gene expression differences to be shown. The relatively few differences between *Mlx*KO and DKO expression profiles (Figure 3*D* and insert) was consistent with the notion that, at least in the normal nonproliferating liver, the Mlx Network contributes more to regulating both the direct and indirect

targets of both networks. The differences between the DKO vs *Mlx*KO groups in Figure 3*D* thus were comparable with those between WT and *Myc*KO groups shown in Figure 3*C*.

IPA profiling of the differentially expressed transcripts in DKO livers (and by extension *Mlx*KO livers) showed that 6 of the top 7 most affected pathways were those with roles in mRNA translation and its control, energy metabolism, and mitochondrial structure and function (Figure 3*E*). The seeming exception (coronavirus pathogenesis pathway) contained numerous ribosomal protein transcripts whose dysregulation accounted for this pathway's inclusion.

Collectively, these findings agreed with previous reports in livers, liver cancers, and other cell types showing roles for the extended Myc pathway in the earlier-described processes.[1,2,13,17,18,24,25,37,47,51–54] Gene expression profiles compiled from the pathways shown in Figure 3E showed the down-regulation of numerous transcripts encoding proteins involved in translation and mitochondrial structure and function in MycKO and MlxKO livers and an even greater degree of down-regulation in DKO livers (Figure 3F and G).[25]

To explore the potential co-regulation of direct target genes by the Myc and Mlx Networks, we obtained data from the most current version of the Encyclopedia of DNA Elements database (https://www.encodeproject.org)[55] and focused on the HepG2 HCC cell line, which was deemed the most relevant to the current work. CRISPR editing had inserted in-frame 3xFLAG epitope tags into the 3' end of the endogenous MYC or MLX coding regions, thus allowing all Chromatin immunoprecipitation (ChIP) sequencing studies to be performed under identical conditions with the same anti-FLAG antibody. The results were trimmed using a default setting that enumerated only those binding sites within ±2.5 kb of the transcriptional start site of each gene, thereby maximizing the likelihood of functional relevance. In this way, we identified 4152 genes that bound only Myc, 748 that bound only Mlx, and 2433 that bound both factors at 6047 sites, 5267 of which overlapped, either entirely or partially (Figure 3H). Thirty-seven percent of Myc target genes (2433 of 6558) also bound Mlx, whereas 76% of Mlx target genes (2433 of 3181) also bound Myc, thus indicating that Mlx target genes are twice as likely to also bind Myc. Fifty percent of the Myc and Mlx binding site peaks mapped to within 65 bp of one another and 75% mapped to within 170 bp, thus indicating that the 2 factors either bound to the same E-box or ChoRE, or to more than 1 element in such close proximity that their individual peaks could not be resolved simply by examining the ChIP sequencing footprints (Figure 3I).

To confirm the earlier-described results and obtain greater resolution and characterization of Myc and Mlx binding, we analyzed the sequences flanking the sites of maximum factor binding (ie, the ChIPseq binding peaks). The earlier-described 6047 binding sites were merged to 2863 distinct sites for motif analysis. A total of 1220 of these (42.6%) contained consensus E-boxes for Myc–Max and 714 contained consensus ChoREs[56] (Figure 3J). A total of 45.2% of the sites contained neither E-boxes nor ChoREs, despite the presence of prominent Myc and/or Mlx footprints, thereby indicating either that the motifs did not conform to the conservative consensus sequences used in our search or that Myc and Mlx binding was indirect as a result of association with other DNA binding factors.

Remarkably, the E-boxes and ChoREs in Figure 3J showed a nonrandom distribution and tended to reside within close proximity of factor-binding peaks. The consensus binding sites located closest to or at the peak centers tended to be those whose adjacent sequences contained either the fewest numbers of additional motifs or tightly clustered ones. This suggested that many ChIP

sequencing peaks represent the integrated signal of multiple variably overlapping and unresolvable individual binding sites and thus do not necessarily directly overlie a particular site. Collectively, these findings confirm the presence of multiple E-boxes and/or ChoREs within the majority of common target genes as well as direct evidence of Myc's binding to ChoREs and Mlx's binding to E-boxes in select cases. They further suggest a means by which the apposition of multiple binding sites within some genes could allow for the simultaneous binding of different combinations of factors as well as their direct interaction and crosstalk.

Cataloging the functions of the 2433 common genes shown in Figure 3H using the IPA and MitoProteome databases and a bespoke collection of previously published genes[25,51,57,58] showed that many could be categorized as supporting mitochondrial and ribosomal structure and function (Figure 3K).[25,57] Thus, the common Myc- and Mlx-bound target genes in human HepG2 cells faithfully reflect both the current transcript changes and those previously documented in MycKO and/or ChrebKO murine livers and hepatoblastomas.[25,57] Interestingly, the 4152 genes bound only by Myc and the 748 genes bound only by Mlx were in somewhat different IPA categories than the common genes (Figure 3K). For example, Myc-specific genes also were involved in more restricted and/or unique functions such as transforming growth factor-β signaling, cell cycle, and oxidative phosphorylation. Similarly, Mlx-specific genes also tended to belong to distinct functional categories such as those related to retinoic acid signaling, xenobiotic metabolism, fatty acid β-oxidation, and the tricarboxylic acid (TCA) cycle.

Given the extended Myc Network's dynamic nature (Figure 2A), the potential for different members to bind multiple closely neighboring sites with different affinities (Figure 3J), and their ability to either augment or antagonize one another's transcriptional impact, we hypothesized that Myc and Mlx binding alone (Figure 3I and J) would not necessarily predict target gene expression levels. We further hypothesized that the transcriptional impact on any individual target gene ultimately would reflect the entire extended network's integrated action.[59] We thus examined the expression of the 2433 common Myc and Mlx target genes (Figure 3H) in 371 human HCCs using data from The Cancer Genome Atlas. Target gene expression could be categorized into 4 groups (designated A–D) that correlated with 4 patterns of extended Myc Network member expression (groups 1–4) (Figure 3L). Two of the tumor groups also showed significant differences in survival (Figure 3M). Together with the results of Figure 3J, these findings support the idea that the binding of Myc, Mlx, or any other extended Myc Network factor to a target gene likely reflects only 1 aspect of the complex and integrative interplay among other network members that collectively dictates the gene's expression level and downstream biological consequences.[20]

Myc, particularly when it is overexpressed by tumor cells, promotes the Warburg effect by up-regulating genes encoding glucose transporters and glycolytic enzymes.[12,25,40,53,60–65] However, none of these showed altered expression in MycKO livers (Table 3). In contrast, the
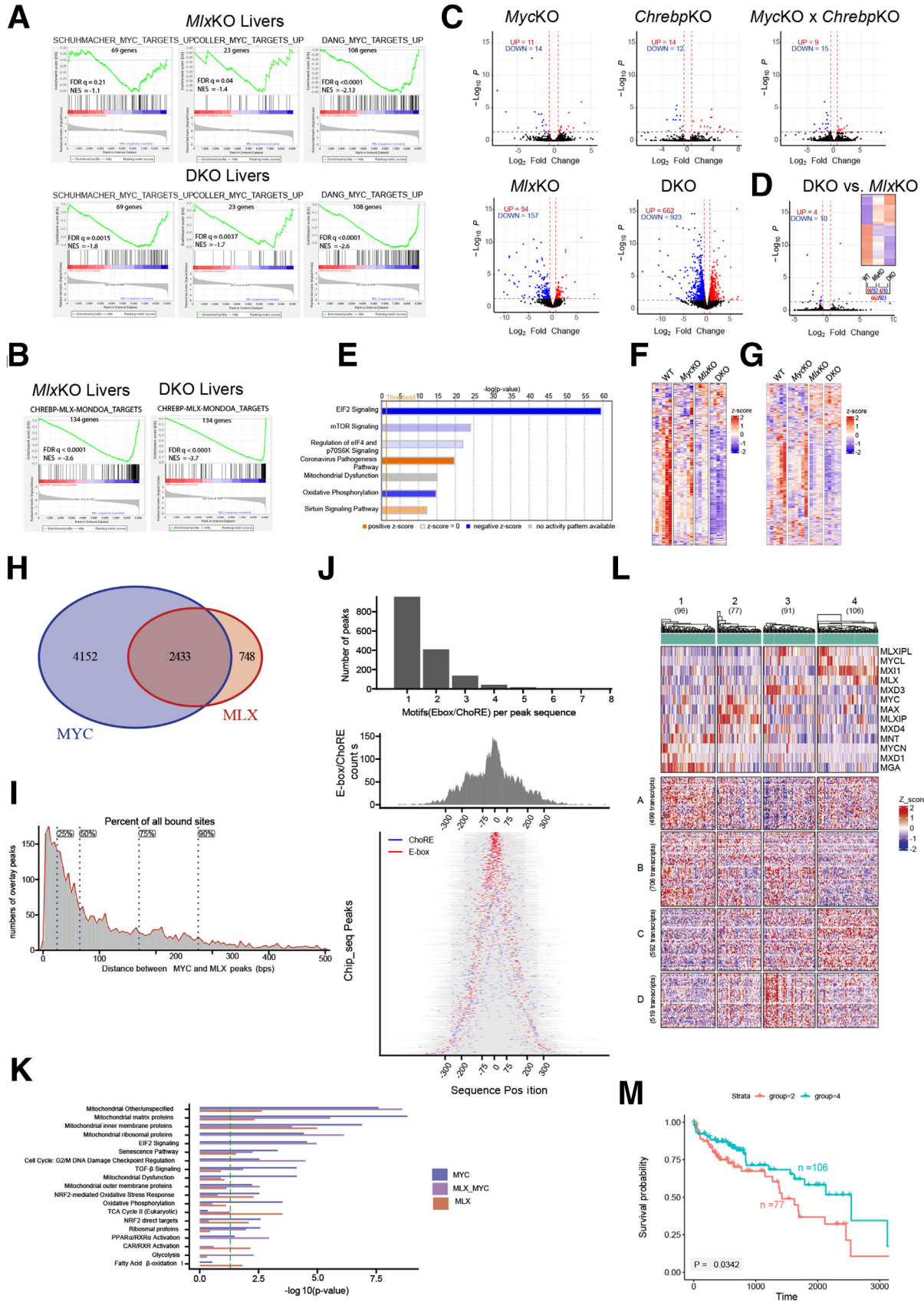
Table 3. Relative Expression Levels of Transcripts for Rate-Limiting Factors in the Glycolytic Pathway

Liver genotype	Glucose transporter 2 (Slc2a2)	Phosphofructokinase-liver type (Pfkl)	Pyruvate kinase L/R (Pklr)
WT	1.00	1.00	1.00
*Myc*KO	1.19 (q = 1)	0.89 (q = 1)	1.62 (q = 0.66)
*Chrebp*KO	0.30 (q = 5.0×10^{-5})	1.07 (q = 1)	0.30 (q = 2.0×10^{-7})
*Myc*KO × *Chrebp*KO	0.41 (q = 0.02)	0.95 (q = 1)	0.29 (q = 7.0×10^{-8})
*Mlx*KO	0.10 (q = 8.3×10^{-10})	0.81 (q = 0.44)	0.19 (q = 1.0×10^{-10})
DKO	0.13 (q = 3.9×10^{-9})	0.63 (q = 0.01)	0.16 (q = 2.4×10^{-15})

progressive inactivation of the extended Myc Network was associated with the down-regulation of 3 transcripts encoding rate-limiting transporters or enzymes, including the major hepatocyte glucose transporter Glut2/Slc2a2 and the glycolytic enzymes liver-type phosphofructokinase (Pfkl) and liver-type pyruvate kinase (Pklr). Glut2/Slc2a2 also is required for the proper regulation of glucose-sensitive genes and for glucose-stimulated insulin secretion.[64,66] These findings were consistent with the previous IPA showing that genes comprising a glycolysis-related set were co-bound by Myc and Mlx (Figure 3K).

Loss of the Extended Myc Network Members Causes Steatosis

Consistent with findings that the Myc and Mlx Networks both impact pathways involved in carbohydrate and lipid metabolism (Figure 3K),[1,2,7,24,25,37,67,68] young *Myc*KO, *Chrebp*KO, and *Myc*KO × *Chrebp*KO mice develop steatosis.[25,37,69] However, these studies did not determine if this was progressive or if the dual compromise of the Myc and Mlx Networks increased its severity. We therefore examined the livers of older (14–16 mo) *Myc*KO, *Chrebp*KO, *Myc*KO × *Chrebp*KO, *Mlx*KO, and DKO mice to evaluate the extent of lipid imbalance. Relative to WT livers, all KO livers showed more intense Oil Red O staining but did not differ significantly from one another (Figure 4A–F). They also contained more total triglycerides than livers from younger *Myc*KO, *Chrebp*KO, and *Myc*KO × *Chrebp*KO mice[25,37] (Figure 4G). These findings suggest that steatosis appears earlier in *Mlx*KO and DKO mice, with *Myc*KO mice eventually achieving a similar degree of severity.

In further support of the earlier-described conclusions, we also found evidence for enrichment of a 163-member gene set

Figure 3. (*See previous page*). **Transcriptional dysregulation in response to Myc and/or Mlx Network inactivation.** (*A*) Gene set enrichment analysis (GSEA) performed on RNA sequencing data sets obtained from *MlxKO* and DKO livers. Three sets of direct Myc target genes from the MSigDB collection containing 69, 23, and 108 members, respectively, were used in the analysis, with expression levels compared with those of WT livers (N = 5 samples per group). (*B*) A 154-member collection of direct MondoA, ChREBP, and Mlx target genes from the Qiagen IPA data set was used in GSEA on the samples shown in panel *A* (Table 2). (*C*) Volcano plots of differentially expressed genes in the indicated livers expressed relative to WT livers. *Red dots*, up-regulated; *blue dots*, down-regulated relative to WT livers. *Chrebp*KO and *Myc*KO × *Chrebk*KO liver RNA sequencing results were obtained from Wang et al.[25] (*D*) Comparison of *MlxKO* and DKO livers showing the differential expression of only 14 transcripts. *Inset*: Heat map of differentially expressed transcripts among WT, *MlxKO*, and DKO livers. (*E*) IPA analysis showing the top 7 dysregulated pathways in DKO livers. (*F*) Heat maps of expression differences for 260 transcripts from the MSigDB C2 database encoding ribosomal subunits and proteins involved in translation (https://www.gsea-msigdb.org/gsea/msigdb/cards/REACTOME_TRANSLATION). (*G*) Expression differences for 605 transcripts encoding proteins comprising the mitochondrial proteome were compiled from the MitiProteome database (http://www.mitoproteome.org). (*H*) Myc and Mlx binding sites in HepG2 cells. ChIP sequencing results were downloaded from the Encyclopedia of DNA Elements database (https://www.encodeproject.org) and analyzed for consensus Myc and Mlx binding sites residing within ±2.5 kb of transcriptional start sites. The Venn diagram shows genes that bound only Myc, only Mlx, or both factors. (*I*) Proximity of Myc and Mlx binding sites within the common target genes shown in panel *H*. Of the 2433 genes shown, a total of 5267 Myc and Mlx binding sites with overlapping footprints were identified. The positions corresponding to the peak center for each factor and the distances between them were determined. (*J*) The location and identities of E-boxes and ChoREs in relation to each factor's binding site peaks. *Top*: Number of E-boxes and/or ChoREs associated with each footprint. *Middle*: Proximity of all motifs in relation to their site peak centers (designated as 0). *Bottom*: Actual location of E-box and ChoRE motifs in each fragment and their position relative to the peak centers. *Gray bars* correspond to the length (in base pairs) of sequences that were determined. Some genes are depicted more than once because they contained more than a single nonoverlapping binding site. (*K*) Select functional categories of genes represented by each of the 3 subsets of genes depicted in panel *H*. *Green dotted line*: $P < .05$. (*L*) The transcriptomes (HTSeq-FPKM-UQ files) of 371 primary HCCs from The Cancer Genome Atlas (TCGA) were downloaded using the TCGAbiolinks R package[49] and then assigned to 1 of 4 groups (1–4) based on the expression of the indicated members of the extended Myc Network determined using the ComplexHeatmap R package.[50] Tumors within these groups could be assigned to 4 additional categories (A–D) based on the expression patterns of the common 2433 transcripts shown in panel *H*. A total of 116 of the genes are not shown because their expression was not reported in the TCGA database. (*M*) Comparative survival of individuals from groups 2 and 4 in panel *L*.
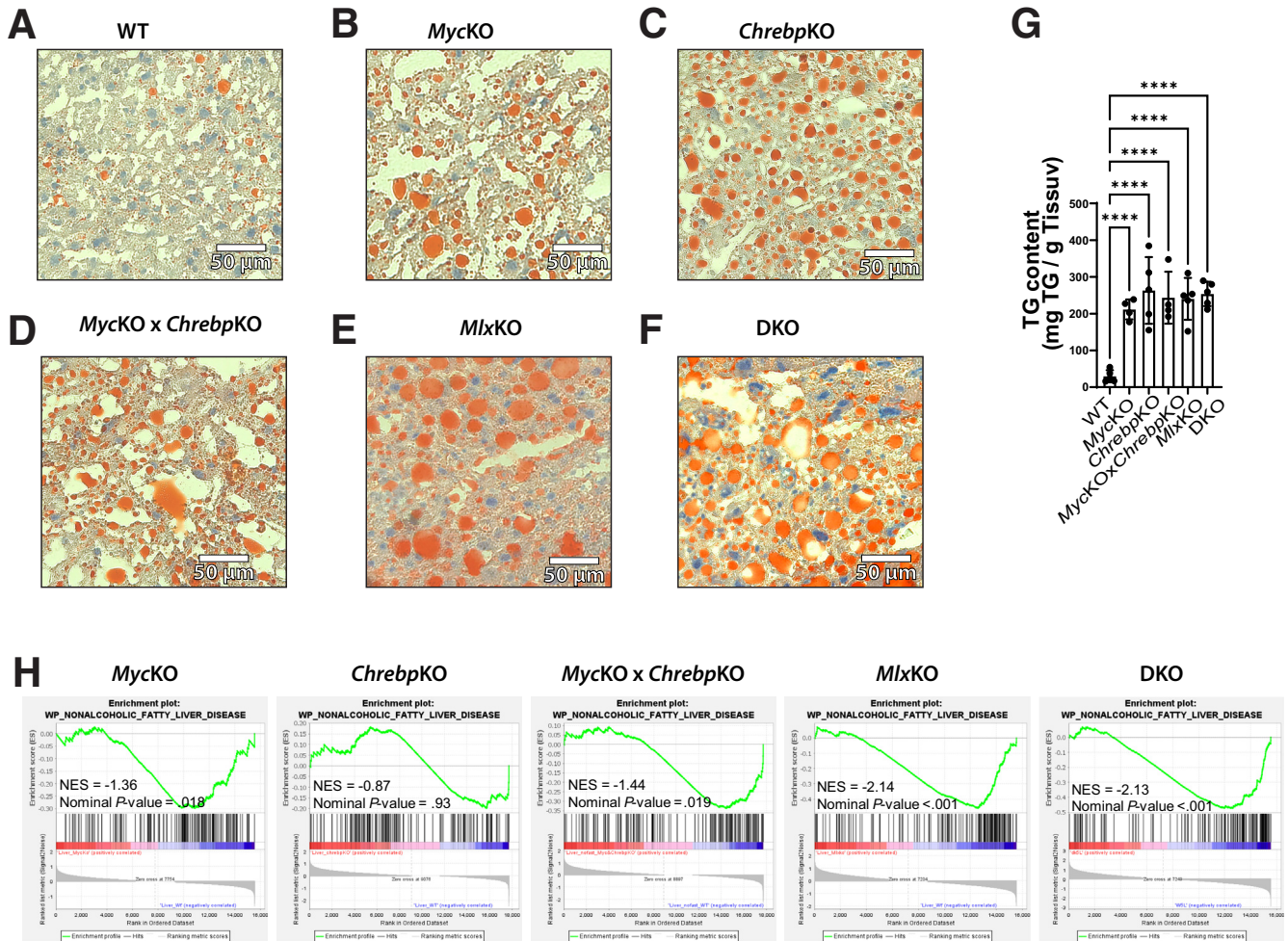
Figure 4. Neutral lipid accumulation is a feature of livers with compromise of the extended Myc Network. (*A–F*) Oil Red O–stained sections of livers from mice ages 14–16 months of the indicated genotypes. (*G*) Quantification of triglyceride levels in liver samples from panels *A–F*. (*H*) Enrichment of genes involved in human NAFLD. RNA sequencing results from the indicated groups of KO mice were compared with their age-matched WT counterparts for the expression of a gene set involved in NAFLD (https://www.wikipathways.org/instance/WP4396_r98945). Normalized enrichment scores (NES) and nominal *P* values are shown above each profile.

associated with human nonalcoholic fatty liver disease (NAFLD) in all cohorts except *Chrebp*KO (https://www.wikipathways.org/instance/WP4396_r98945) (Figure 4*H*). Thus, despite the fact that the causes of steatosis in the earlier-described mice and human beings differ considerably, in most cases there is considerable similarity in the disease-related gene expression profiles.[70]

Finally, we performed IPA to identify additional disease-related pathways that sometimes are dysregulated in NAFLD[70] and in all cases found several relating to lipid synthesis/metabolism and peroxisome proliferator-activated receptor(PPAR) activation (Table 4). While noting little histologic evidence for inflammatory cell infiltrates or fibrosis in our KO livers, several of these pathways were in fact associated with nonalcoholic steatohepatitis (NASH) (Table 4). Although these transcriptome-based findings may represent early evidence of actual NASH, the altered expression of inflammatory markers also could be indicative

of the immune function changes that accompany Myc dysregulation in nonhepatic tissues.[37,71] We believe the most conservative interpretation of the earlier-described results is that the steatosis accompanying the loss of most extended Myc Network members is progressive and eventually leads to a mild NASH-like picture as indicated by significantly altered molecular markers of this state, but little documentable histopathologic change.

*Mlx*KO and DKO Mice Develop Age-Related Hepatic Adenomatosis and Occasional HCC

Unexpectedly, 36% of *Mxl*KO and DKO animals (15 of 42) of both sexes developed multiple small- to medium-sized hepatic neoplasms, which were never observed in WT, *Myc*KO, *Chrebp*KO, or *Myc*KO × *Chrebp*KO mice (Figure 5*A* and *B*).[25,37] These were mostly well-differentiated and/or myxoid-type tumors with numerous

Table 4. IPA Profiling of KO Livers

IPA diseases and functions	Cohort	P value
Activation of PPAR in Liver cells	MycKO	<.01
	ChrebpKO	<.01
	MycKO × ChrebpKO	<.01
	MlxKO	<.01
	DKO	<.01
Lipid synthesis	MycKO	$<10^{-5}$
	ChrebpKO	$<10^{-5}$
	MycKO × ChrebpKO	$<10^{-5}$
	MlxKO	$<10^{-5}$
	DKO	$<10^{-5}$
Fatty acid metabolism	MycKO	$<10^{-5}$
	ChrebpKO	$<10^{-5}$
	MycKO × ChrebpKO	$<10^{-5}$
	MlxKO	$<10^{-5}$
	DKO	$<10^{-5}$
Liver inflammation	MycKO	<.01
	ChrebpKO	<.01
	MycKO × ChrebpKO	<.01
	MlxKO	<.01
	DKO	<.01
Fibrosis of the liver	MycKO	<.01
	ChrebpKO	<.01
	MycKO × ChrebpKO	<.01
	MlxKO	<.01
	DKO	<.01
Hepatic steatosis	MycKO	<.01
	ChrebpKO	<.01
	MycKO × ChrebpKO	<.01
	MlxKO	<.01
	DKO	<.01

NOTE. Relevant NAFLD-associated IPA in livers from the indicated KO groups compared with WT livers. Because so few gene expression differences existed in MycKO, ChrebpKO, and MycKO × ChrebpKO livers (Figure 3C), the criteria for differential expression were relaxed to include those genes with more than 1.2-fold differences and P values < .05.

balloon cells, nuclear enlargement, and microvesicular steatosis. A minority also showed small foci of well-differentiated HCC, which sometimes is associated with hepatic adenomas in human beings (Figure 5C).[44,72] Regardless of histology, adenomas showed significantly more staining for Ki-67 than did the adjacent non-neoplastic liver parenchyma (Figure 5D) ($P = 3.4 \times 10^{-5}$).

Adenomas did not express Mlx protein, indicating that they did not originate from residual hepatocytes that had escaped Mlx locus excision and maintained their growth advantage (Figure 5E). Normal livers and DKO adenomas also did not express detectable Myc protein, and neither did most MlxKO adenomas. This was consistent with their slow growth rates and a likely consequence of their extended Myc Network defects (Figure 3C–G).[25,37] An exception was seen in a single large adenoma containing elements of HCC from an MlxKO mouse with marked hepatomegaly (liver weight, 6.7 g, or approximately 3 times normal) (Figure 5E). We performed RNA sequencing on 5 adenomas from MlxKO mice and compared their transcriptome profiles with those of WT livers and 45 primary murine hepatoblastomas (HBs) generated by overexpressing the Hippo pathway terminal effector yes-associated protein (YAP[S127A]) and 1 of 9 different patient-derived oncogenic mutants of β-catenin.[73] The transcriptional profiles of the adenomas were distinct from those of both livers and all HBs (Figure 5F and G). Adenomas did not overexpress wild-type β-catenin or YAP as is common for HBs,[74] but did dysregulate 15 of 22 transcripts that are expressed aberrantly in all murine HBs regardless of etiology and that correlate with survival in human HB and other cancers (Figure 5H).[47,75] Our results indicate that dismantling the Mlx Network, either alone or concurrently with Myc, leads to the eventual emergence of multiple adenoma-like hepatic neoplasms (adenomatosis), which, similar to their human counterparts, may evolve further and acquire HCC-like features.[72]

Discussion

Most previous investigations into Myc's role in hepatic regeneration have relied on the PH model and yielded conflicting results that likely reflected differences in how and when regeneration was assessed and quantified.[37] The short time frame over which this process occurs and the dependency on separate groups of mice may have further contributed to disparate outcomes. Because post-PH hepatocytes require fewer than 2 divisions to replace the missing mass, the model also poses a comparatively modest regenerative challenge. Indeed, even this low number overestimates the actual contribution made by dividing hepatocytes given that approximately half the response to PH involves hypertrophy of the liver remnant plus replicative contributions by nonhepatocyte populations such as endothelial, Kupfer, and stellate cells.[38,76,77] In contrast, the FAH model is associated with a more sustained and robust 50- to 100-fold expansion of pure populations of transplanted hepatocytes. It also provides a well-defined point at which a stable level of regeneration can be assessed and a means by which competing donor populations within the same liver can be simultaneously distinguished and quantified after their delivery at any desired and preselected ratio.[25,37,52] Using this approach, we previously showed that the long-term proliferation of otherwise normal hepatocytes requires ChREBP but not Myc, although the loss of both factors was additive.[25,37] Even more pronounced interdependencies were seen during HB tumorigenesis, with HB growth impaired markedly in both MycKO and ChrebpKO livers, and even more so in MycKO × ChrebpKO livers.[25,46,47] These findings implied a means of communication between the Myc and Mlx Networks, with each one being able to rescue, at least partially, defects in the other.[1] They also showed that the requirement for Myc becomes progressively more critical as proliferative demand increases, thus emphasizing its strong contextual dependency (Figure 6).

Despite our previous transplant studies having been performed with different input ratios of WT and KO hepatocytes,[25,37] their outcomes were consistent with those reported here and allowed us to extend our conclusions regarding the relative importance of the Myc and Mlx
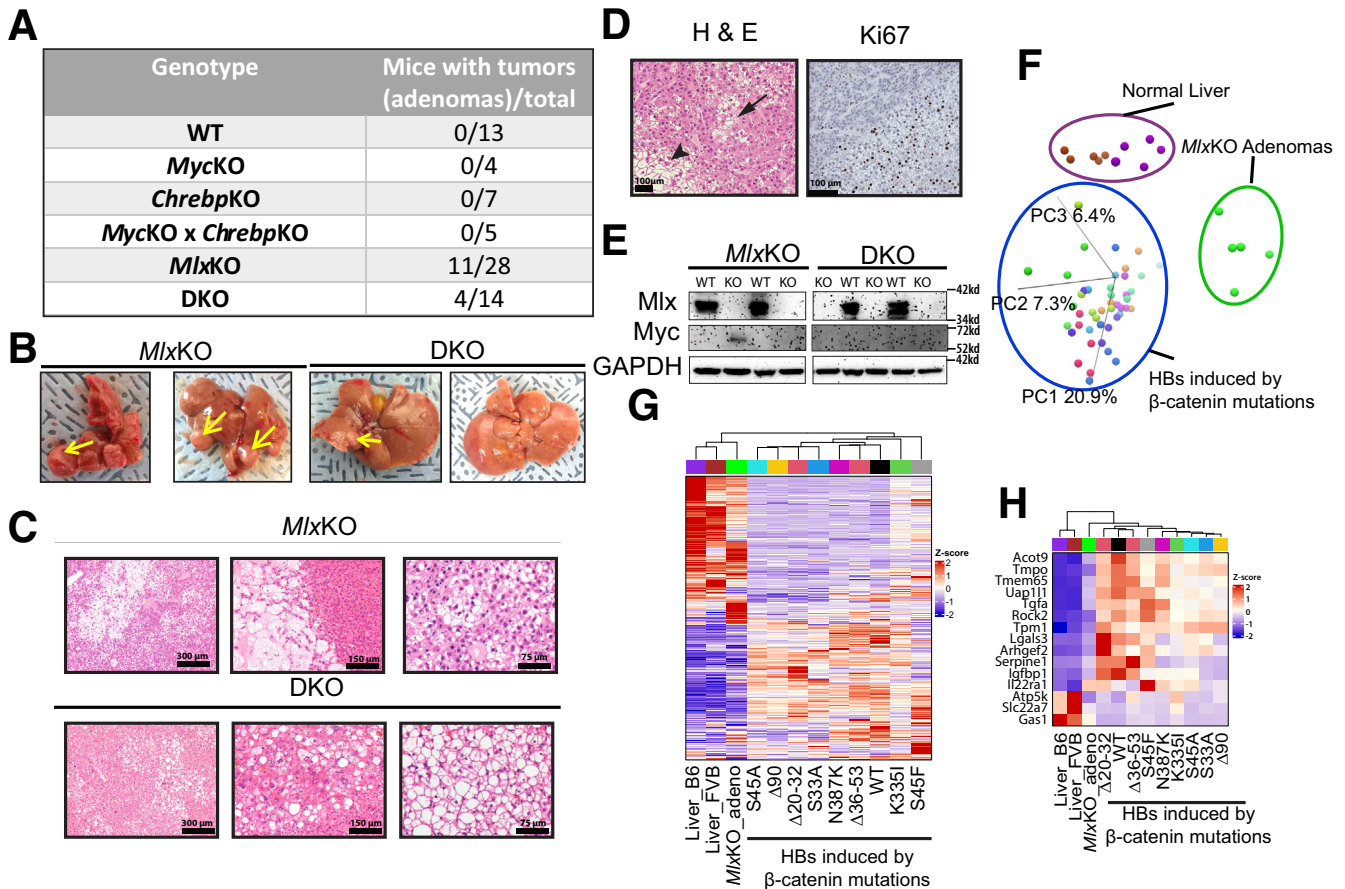
Figure 5. Characterization of hepatic adenomas originating in *Mlx*KO and DKO livers. (*A*) Number of mice ages 14–16 months of the indicated genotypes with visible liver tumors at the time of death. (*B*) Gross appearance of tumor-containing livers from panel *A*. Tumors were generally small but multifocal (*arrows*). (*C*) H&E-stained sections showing the typical appearance of *Mlx*KO and DKO livers. The first 2 *Mlx*KO images show well-differentiated and myxoid-type adenomas, respectively, whereas the third panel shows a focus of well-differentiated HCC embedded within an adenoma. The first 2 DKO images show regions of microvesicular steatosis with balloon cells and nuclear enlargement, respectively, whereas the third image shows another adenoma that is quite similar in appearance to those arising in *Mlx*KO livers. (*D*) H&E and Ki-67 immunostained sections of the Myc-expressing adenoma from panel D showing regions of inflammation (*arrowhead*), adjacent to those resembling well-differentiated HCC (*arrow*). Ki-67 staining is more intense within the nodular adenoma (*lower right*) compared with adjacent normal liver (*upper left*). Quantification of Ki-67 staining from 4 different adenomas and adjacent normal tissue was performed on 300–2000 cells from each region. The mean Ki-67 index in adenomas was 30.08% $\pm$ 6.5% vs 3.2% $\pm$ 3.1% in adjacent nonadenomatous tissues ($P = 3.4 \times 10^{-5}$). (*E*) Immunoblots showing Mlx expression in WT livers and its absence in adenomas arising from *Mlx*KO and DKO livers. Only 1 large adenoma from an *Mlx*KO mouse with hepatomegaly expressed detectable levels of Myc (*lane 2*). (*F*) Principal components analysis (PCA) of whole transcriptomes from WT livers, HBs generated by the overexpression of mutant forms of β-catenin+YAP^{S127A}, and the earlier-described adenomas. (*G*) Whole-transcriptome profiles of the tissues from panel *F*. Note that control liver samples were derived from 2 different strains: C57B6 and FVB. (*H*) Heat maps of 15 of the 22 transcripts that are dysregulated in murine HBs and correlate with poor outcomes in human HBs and other human cancers.[47] GAPDH, glyceraldehyde-3-phosphate dehydrogenase; PC, Principal Component.

Networks in liver regeneration. For example, our studies comparing WT and *Chrebp*KO hepatocytes used an input inoculum comprising 62% of the latter population that was reduced by more than half after competitive repopulation.[25] Our current results in which *Mlx*KO hepatocytes comprised approximately 84% of donor cells but only approximately 4% of the final population (Figure 2*D*) provided strong evidence that the concurrent functional inactivation of both ChREBP and MondoA confers an even more profound proliferative disadvantage. This could be a direct effect resulting

from the concurrent loss of ChREBP and MondoA binding to their respective target genes, either individually or collaboratively with Myc, thereby eliminating any possibility of rescue of 1 factor by another (Figure 2*A*).[24,26–29] A non-mutually exclusive indirect effect that allowed Mxd1, Mxd4, and Mnt to suppress Myc target genes more effectively by increasing their association with Max also remains possible (Figure 2*A*). The relative importance of these 2 models could vary among different target genes at different times during repopulation or in different liver compartments.
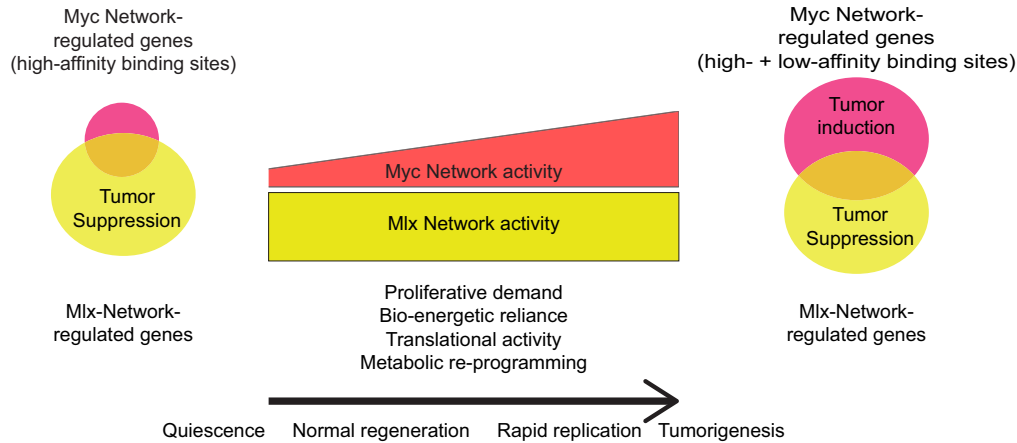
Figure 6. A model for gene regulation and control of normal and neoplastic proliferation by the extended Myc Network.
During quiescence, Myc levels are low and its target genes, which are relatively few in number (Figure 3 and Hofmann et al[78]), tend to be those with high-affinity E-box binding sites. Slow and controlled replication, such as that occurring during the replacement of *Fah-/-* hepatocytes, is largely regulated via the Mlx Network.[25,37] As replication increases or as cells acquire transformed features, increased Myc expression[25,51] activates genes with low-affinity binding sites, including those encoding glycolytic enzymes that collectively are responsible for the Warburg effect as well as other metabolic pathways and functions that support increased energy demands and rapid growth.[2,3,24,40,53,65,69,79] Despite the rapid growth that occurs in response to the overexpression of Myc and mutant forms of β-catenin and YAP^{S127A}.[25,51,73] The Mlx Network, which supports this rapid growth, is proposed to contribute to tumor suppression as well (Figure 5).

We also previously showed that the combined loss of *Myc* and *ChREBP* suppressed regeneration more than the KO of either individual gene, thereby corroborating previous evidence for internetwork crosstalk.[2,3,13,24,25] In 1 such study, performed with nearly equal contributions of WT and *Myc*KO × *Chrebp*KO donor hepatocytes, the latter was reduced to 7.5% after repopulation.[25] Although impaired markedly, the residual proliferative activity of these cells could have reflected the redundant function of MondoA (Figure 2A), which is supported by 2 separate aspects of the current work. The first was the approximately 45-fold repopulation advantage of WT hepatocytes over DKO hepatocytes, whereas the second was the approximately 10-fold repopulation advantage of *Mlx*KO hepatocytes over DKO hepatocytes (Figure 2F and H). Collectively, our current results indicate that both the Myc and Mlx Networks play distinct as well as redundant roles in normal hepatocyte replication. However, much of the proliferative drive needed to sustain hepatocyte expansion in FAH mice is subsumed by the Mlx Network regardless of the Myc Network's status.[25,37] This is supported by the progressive deterioration of repopulation potential as the Extended Network is gradually dismantled (Figure 2C–H).[25]

In proliferatively quiescent cells or organs such as the liver, Myc usually is expressed at low levels and regulates relatively few genes in contrast to Mlx (Figures 3C and 5E).[25,37,78] Myc's contribution to genome-wide transcription therefore may be better appreciated in tumors where its overexpression can activate genes that are otherwise non-physiologic targets owing to their low-affinity binding sites.[10,11,25,68] Another plausible explanation for the seemingly modest transcriptional consequences of Myc loss in some normal tissues is that at least some Myc target gene expression is maintained by the Mlx Network with redundant contributions being made by MondoA and/or ChREBP.[25,37,78] This is best appreciated in livers and tumors when the Myc and Mlx Networks are either individually or concurrently inactivated (Figure 3C).[25]

In tumors, the Myc Network positively regulates most of the genes encoding glycolytic enzymes and strongly contributes to the Warburg effect,[5,12,40,51,53,61,65,80] as it does in rapidly growing fibroblasts in vitro.[40,80] In contrast, our transcriptomic studies have not shown such widespread roles for the Myc and Mlx Networks in maintaining glycolysis in vivo (Table 3 and Figure 3K), which may reflect Myc's low-level expression, the relative proliferative quiescence of the normal liver, and its greater reliance on fatty acid oxidation as an energy source.[25,46,51,73] Nonetheless, among the most down-regulated genes in *Mlx*KO and/or DKO livers were *Glut2/Slc2a2*, *Pfkl*, and *Pklr*, whose encoded proteins are rate-limiting for glucose uptake and glycolysis. In rat insulinoma cells, the *Pklr* proximal promoter binds both ChREBP and Myc, with the former interacting with a ChoRE element and the latter binding elsewhere.[28,29] These results suggest that, in normal liver, glucose uptake and oxidation are more reliant on the Mlx Network (Figure 6) whereas, in response to Myc-driven transformation or normal proliferation, more extensive transcriptional regulation of glucose uptake and its oxidation is achievable.[4,14,23,25,51,81] This could have the additional benefit of maximizing glycolytic efficiency and sustaining cell division when microenvironmental glucose and oxygen supplies were limiting and nutrient-dependent functions of MondoA and ChREBP were attenuated.[82]

Coordinated changes in direct and/or functionally related Myc and Mlx Network target genes were identified in *Mlx*KO and DKO livers but were more pronounced in the latter (Figure 3A–D).[25,37] Some have been shown previously

to support protein translation and its control as well as mitochondrial structure and function (Figure 3E–G).[18,25,37,40,51,69,73] As was seen for individual glycolysis-related transcripts (Table 3), the collective expression of these sets became increasingly compromised as the extended Myc Network was progressively inactivated. The dramatic up-regulation of these pathways that accompanies tumorigenesis in WT livers also had been shown to be attenuated in response to Myc and/or ChREBP inactivation and to correlate with impaired rates of tumor growth.[25] We provided a mechanistic underpinning for the coordinated response of the relevant gene sets associated with these pathways by showing that, in HepG2 cells, 37% of Myc's direct target genes also bind Mlx, while 76% of direct Mlx target genes also bind Myc (Figure 3H). Many of the previously mapped binding sites for these 2 factors overlapped and/or contained multiple E-boxes and/or ChoREs (Figure 3I and J). Although this sometimes made it difficult to attribute Myc or Mlx binding precisely to a specific motif within a factor's ChIP sequencing footprint, the collective binding landscape suggested a model for target gene regulation that accommodates this and all other observations. The model accounts for the fact that many sites containing only E-boxes coincided with Mlx binding peaks whereas many ChoRE-only sites coincided with Myc binding peaks (Figure 3J). This indicated that crosstalk between the Myc and Mlx Networks occurs by virtue of shared common binding sites as previously suggested. The nonrandom distribution of E-boxes and ChoREs around Myc and Mlx binding peaks (Figure 3J) also suggests that more than one such site could be occupied at any given time, that binding might be cooperative, and that the composition of the bound factors, their interactions, with each other and differential protein–DNA affinities are dynamic and serve to fine-tune the target gene's transcriptional output. Although we examined only Myc and Mlx binding, these motifs also could bind other extended Myc Network members such as those between Max and Mxd proteins, which would not have been detected with our ChIP sequencing analysis. Whether closely spaced Mlx sites contained ChREBP or MondoA heterodimers also potentially could determine if, when, and the degree to which a gene was responsive to metabolic substrate-mediated regulation. Finally, the 4 groups into which the expression patterns of the 2433 common Myc + Mlx direct target genes in HCCs could be compiled correlated with the patterns of extended Myc Network transcript expression and, in 2 cases, with significant survival differences (Figure 3L and M). In future studies, it will be important to determine the degree to which different neighboring heterodimeric combinations of extended Myc Network members either cooperate with or antagonize one another under different conditions in different cell types.

Myc and/or ChREBP inhibition are widely associated with lipid accumulation, which stems from an over-reliance on fatty acid oxidation and a resulting increase in lipid uptake that exceeds the amount necessary to satisfy energy demands (Figure 4).[25,37,67,83,84] Young mice with hepatocyte-specific loss of *Chrebp* or combined *Myc* + *Chrebp* loss also accumulate more neutral lipids than do those with isolated Myc loss.[25] Although we did not serially follow these animals, our findings suggest that, early in life, the partial or complete inactivation of the Mlx Network promotes a more rapid genesis of steatosis than inactivation of Myc alone. Over time, however, lipid accumulation equalizes, with little differences among the various KO groups being discernible in older individuals (Figure 4G). KO livers dysregulated many of the same gene sets and/or IPA pathways that have been described in NAFLD and its progression in human beings (Figure 4H and Table 4), thereby further supporting the mechanistic relatedness of the various factors responsible for this state. Because KO livers also showed molecular evidence of incipient NASH, it will be important in future work to determine whether these features become more pronounced with age and whether histologic findings of inflammation and fibrosis eventually emerge.[85,86]

An unanticipated finding was the development of hepatic adenomatosis in more than one third of *Mlx*KO and DKO mice (Figure 5A and B). This incidence likely represents an underestimate because animals older than 14–16 months were not investigated and microscopic adenomas may have been overlooked in some instances. That similar neoplasms did not appear in WT, *Myc*KO, *Chrebp*KO, or *Myc*KO × *Chrebp*KO mice makes it likely that complete Mlx Network inactivation is a prerequisite for their development. Although these neoplasms bear the hallmarks of actual human adenomas,[44,72] several features suggest more aggressive and malignant predilections, despite the lack of Myc expression in most. These include their multifocality, their occasional HCC-like features, and their robust Ki-67 expression (Figure 5C and D). In contrast, human adenomas, although well known for their occasional conversion to HCC, typically are few in number and tend to show only modestly higher Ki-67 expression.[72] Molecular features suggestive of more aggressive behavior in our adenomas include the dysregulation of 15 of 22 transcripts that we recently identified as predicting inferior outcomes in human HBs and more than a dozen other human cancer types (Figure 5H).[47]

Recurrent *MLX* gene deletions are associated with at least 8 human cancer types and provide further reason to implicate the Mlx Network in the pathogenesis of hepatic adenomatosis (https://portal.gdc.cancer.gov/genes/ENSG00000108788).[20] Genetic suppressors of hepatic adenomas and other benign tumors such as meningiomas, neurofibromas, and uterine fibroids are well documented but are distinct from more notorious counterparts such as *TP53*, *RB*, *PTEN*, *APC*, and *BRCA1/2* that are associated with malignant tumors.[87–90] However, the role of Mlx and its members also may be more indirect and nuanced. For example, NAFLD (Figure 4) is a known predisposing factor for the development of both adenomas and HCC and we are currently unable to determine how it might affect tumorigenesis in *Mlx*KO mice.[72,91,92] On the other hand, the failure of *Myc*KO, *Chrebp*KO, or *Myc*KO × *Chrebp*KO mice to develop adenomas or HCCs, despite their equally pronounced steatosis as well as the fact that high-fat diets can actually suppress hepatic tumor growth,[93] argues for a more direct

role for the Mlx Network in adenoma suppression. It will be of interest to determine whether *Mlx*KO mice are more susceptible to transformation by other oncogenic stimuli even though the emergence of the ensuing tumors may be delayed and their subsequent growth slowed.

In summary, we have shown that the Mlx Network engages in considerable biological and molecular crosstalk with the Myc Network and plays a more substantive role in long-term liver regeneration.[25,29,35,37,46] Both networks, but the former in particular, alter the expression of numerous genes responsible for broad aspects of translation and energy generation by both aerobic and anaerobic pathways.[25,37,57] The majority of Myc and Mlx targets are co-regulated or at least bound by both factors, which appear to share many of the same binding sites, often lying in close proximity to one another. The actual expression of these target genes further correlates with the expression patterns of all 13 members of the extended Myc Network, thereby suggesting complex interactions and interdependent crosstalk at their sites of binding. Mechanistically, the defects that ensue in KO cells as a result of compromising these genes reflect an inability to maintain energy production and translation at levels commensurate with their proliferative demands. This is particularly acute in the neoplastic setting where tumor growth, but not induction, may be severely compromised.[25,37,57] The presumptive energy dysequilibrium that arises as a consequence of perturbing either or both of the networks likely is addressed by the increased uptake and storage of fatty acids, leading to eventual steatosis.[25,73] The hepatic adenomatosis and occasional HCC seen in response to Mlx Network compromise suggests that the tumor suppressor–like activity of the Mlx Network counters the more pro-oncogenic tendencies of Myc overexpression. Our findings emphasize the elaborate orchestration of the Extended Myc Network in balancing energy demands and metabolism with normal and neoplastic proliferation.

Materials and Methods
Animal Studies

All breeding, care, husbandry, and procedures were approved by The University of Pittsburgh Department of Laboratory and Animal Resources and the Institutional Animal Care and Use Committee, with standard animal chow and water provided ad libitum. C57BL6 mice expressing green fluorescent protein (GFP) (C57BL/6-Tg[UBC-GFP] 30Scha, MGI:3057178) have been described previously and were used as a source of WT control hepatocytes because of the ease with which the *GFP* gene could be identified.[25] C57BL6 *c-myc*[LoxP/LoxP] mice (B6.129S6-Myc[tm2Fwa], MGI:2178233) have been described previously (Figure 1*A*),[25,37,94,95] and were obtained as a gift from I. Moreno de Alboran. The generation of mice bearing a 1717-bp deletion spanning exons 3–6 of the *Mlx* locus (*Mlx*KO mice) (Figure 1*B*) also has been described recently.[8] Transgenic mice expressing a fusion protein comprising the hormone-binding domain of CreER and under the control of the albumin promoter that allows CreER to be activated in

hepatocytes after tamoxifen exposure (B6.129S2- Alb[tm1(cre/ERT2)Mtz] , MGI:3052812) were a kind gift from Dr Frank Gonzalez (Laboratory of Metabolism, Center for Cancer Research, National Cancer Institute). The latter mice were bred to homozygosity with *Mlx*[LoxP/LoxP] mice or *Myc*[LoxP/LoxP] × *Mlx*[LoxP/LoxP] mice.[25,37] At weaning, mice were subjected to 5 daily intraperitoneal injections of tamoxifen (75 mg/kg each) in corn oil (Sigma-Aldrich, St. Louis, MO). Several weeks later, hepatocytes were harvested as previously described.[25,37] An aliquot of these was used for DNA isolation and to quantify the extent of *Myc* and/or *Mlx* knockout (Figure 1). The remainder of the *Myc*KO, *Chrebp*KO, or *Myc*KO × *Chrebp*KO hepatocytes then were combined in the indicated proportions with WT hepatocytes and a total of 3×10^5 cells were injected intrasplenically into *Fah*-/- FRG-NOD mice (Yecuris, Inc., Tualatin, OR)[25,37] (*ChreBP* mice: B6.129S6-Mlxipl[tm1Ku], MGI:3043871; *Fah* mice: NOD.Cg-*Rag1*[tm1Mom] *Fah*[em1Mvw] *Il2rg*[tm1Wjl] MGI:5485380). All animals were maintained on 8 mg/L NTBC (Ark Pharm, Libertyville, IL) in their drinking water. After 4 days, NTBC was discontinued until mice lost approximately 20% of their body weight. NTBC then was reinstated until mice regained their age-appropriate weight. NTBC cycling was continued either until mice had become NTBC-independent (at least 20 weeks after transplantation) or until week 28 in those cases in which NTBC independence was not achieved. Hepatocyte DNAs then were isolated from recipients and the TaqMan-based approaches shown in Table 1 and Figure 1 were used again to determine the donor:recipient ratio and the relative contribution of each donor population.[25,37] Polymerase chain reactions were performed in a volume of 12 μL with 50 ng of genomic DNA. Conditions for amplification were 95°C for 5 minutes, 40 cycles at 95°C for 15 seconds, and 60°C for 60 seconds.

For gene expression profiling, the earlier-described *Myc*[LoxP/LoxP], *Mlx*[LoxP/LoxP], and *Myc*[LoxP/LoxP] × *Mlx*[LoxP/LoxP] mice were bred to B6.129-Gt(*ROSA*)26Sor[tm1(cre/ERT2)Tyj]/J mice (MGI:3699244), which express CreER under the control of the ubiquitously expressed ROSA26 promoter (Jackson Labs, Bar Harbor, ME).[96] Excisional inactivation of each locus was initiated at the time of weaning and confirmed as described earlier. Liver RNAs then were obtained from mice that were the same age as those used for hepatocyte transplants (~5 mo).

Triglyceride Assays

Total lipid was extracted from approximately 50 mg liver using the Folch et al[97] method. Total triglyceride content then was determined as described previously using the Free Triglyceride Reagent (Sigma-Aldrich, Inc).[25,98]

Histology, Immunohistochemistry, and Immunoblotting

Fresh tissues sections were immediately fixed in formalin, embedded in paraffin, and stained with H&E as previously described.[25,37,51] Oil Red O staining and immunohistochemistry on snap-frozen sections also were performed as previously described.[25,37] Tissue samples for

immunoblotting were disrupted in sodium dodecyl sulfate–polyacrylamide gel electrophoresis lysis buffer containing protease and phosphatase inhibitors but lacking β-mercaptoethanol or bromophenol blue as previously described.[25,46,51,73] Protein quantification was performed using the bicinchoninic acid (BCA) reagent according to the supplier's directions (Thermo Fisher Scientific, Rockford, Illinois). After β-mercaptoethanol (1%) and bromophenol blue (10%) addition, samples were boiled for 5 minutes, dispensed into small aliquots, and stored at -80°C until analysis. Sodium dodecyl sulfate–polyacrylamide gel electrophoresis and semidry transfer to PVDF membranes (Sigma-Aldrich) was performed as previously described.[25,46,51,73] Antibodies used for immunoblotting included rabbit monoclonals directed against Mlx and Myc (85570 and 13987; Cell Signaling Technologies, Inc, Danvers, MA) and a mouse monoclonal antibody against glyceraldehyde-3-phosphate dehydrogenase (G8795; Sigma-Aldrich). A mouse monoclonal anti–Ki-67 antibody used for immunohistochemistry also was from Cell Signaling Technologies (#12202). Horseradish-peroxidase secondary antibodies were from Santa Cruz Biotechnology (Santa Cruz, CA). Ki-67 immunostain quantification was performed using the ImageJ Immunohistochemistry Image Analysis Toolbox (https://imagej.nih.gov/ij/plugins/ihc-toolbox/index.html; National Institutes of Health, Bethesda, MD). All antibodies were used at the dilutions recommended by the suppliers. Immunoblots were developed using an enhanced chemiluminescent assay kit as directed by the supplier (SuperSignal West Pico Plus; Thermo-Fisher, Inc, Waltham, MA).

RNA Sequencing and ChIP Sequencing Experiments

RNAs were purified from 5 replica tissues from each group of mice using the Qiagen RNeasy Mini Kit (Qiagen, Inc, Germantown, MD), followed by DNase digestion.[25,37] RNA concentration and integrity was confirmed on an Agilent 2100 Bioanalyzer (Agilent Technologies, Foster City, CA) and only those samples with RIN values greater than 8.5 were used for sequencing. All subsequent analyses were performed as previously described.[25,73] Sample preparation and sequencing was performed on a NovaSeq 600 instrument (Illumina, Inc, San Diego, CA) by Novagene, Inc (Sacramento, CA) and raw data were deposited in the National Center for Biotechnology Information GEO database (accession number: GSE181371). Data sets from previous RNA sequencing studies of *Myc*KO, *Chrebp*KO, and *Myc*KO × *Chrebp*KO livers and mutant forms of β-catenin+YAP^{S127A} HBs are available from the GEO database sets GSE114634 and GSE130178.[25,73] Differential gene expression was assessed by 3 different approaches, namely EdgeR, CLC Genomics Workbench version 21 (Qiagen), and DeSeq2, as previously described.[25,47] When low-abundance reads (counts per million <1) were encountered for both comparisons, they were eliminated. Reads from FASTQ files were mapped to the GRCm38.p6 mouse reference genome using STAR (https://github.com/alexdobin/STAR/releases) version 2.7.5. BAM-formatted output was analyzed and

transcript abundance was determined by featureCounts (http://bioinf.wehi.edu.au/featureCounts). Where necessary, IPA (Qiagen) was used to classify transcripts into pathways whose significance was adjusted for false discovery using the Bonferroni–Hochberg correction. We further used gene set enrichment analysis[48] to identify alterations of functionally related groups of transcripts from the MSigDB C2 collection (v.7.4) (http://www.gsea-msigdb.org/gsea/msigdb/index.jsp) or from the MitoProteome database (http://www.mitoproteome.org). Volcano plots were generated using the R software package ggplot2 (https://ggplot2.tidyverse.org), with significant differences between samples being defined as having fold differences greater than 1.5 and false discovery rates less than 0.05. Heat maps were generated using the ComplexHeatmap package (version 2.6.2; https://bioconductor.org/packages/release/bioc/html/ComplexHeatmap.html). Statistical analyses were performed with R software v4.0.3 (R Foundation for Statistical Computing, Vienna, Austria) and GraphPad Prism v9.00 (GraphPad Software, Inc, San Diego, CA).

To analyze ChIP sequencing data, we explored binding Myc and Mlx to their target gene sequences in 2 different HepG2 cell lines that had been modified using CRISPR so as to introduce 3 × FLAG tags at the C-termini of each protein. This allowed ChIP sequencing to be performed under identical conditions with a single anti-FLAG antibody. The results were downloaded from the Encyclopedia of DNA Elements website (https://www.encodeproject.org) and analyzed using ChIPpeakAnno version 3.13 and the annotation database TxDb.Hsapiens. UCSC.hg38.knownGene (R package version 3.13.0).[99] Only binding sites residing within ±2.5 kb of the transcriptional start of each target gene were considered for the current analysis.[55,100] Overlap between Myc and Mlx binding regions was obtained using the findOverlapsOfPeaks function (set maxgap = 0; minoverlap = 0). Venn diagrams were used to show unique and overlapping binding sites. FIMO (version 5.4.1) from the MEME software suite was used to identify E-boxes and ChoREs most closely associated with ChIP sequencing peaks. Categorization of genes associated with bound peaks was performed using previously described collections of functionally related genes or those from the IPA and MitoProteome databases (Qiagen, Inc, and http://www.mitoproteome.org).

References

1. Carroll PA, Diolaiti D, McFerrin L, Gu H, Djukovic D, Du J, Cheng PF, Anderson S, Ulrich M, Hurley JB, Raftery D, Ayer DE, Eisenman RN. Deregulated Myc requires MondoA/Mlx for metabolic reprogramming and tumorigenesis. Cancer Cell 2015;27:271–285.
2. Carroll PA, Diolaiti D. A novel role for the extended MYC network in cancer cell survival. Mol Cell Oncol 2016;3:e1026528.
3. Carroll PA, Freie BW, Mathsyaraja H, Eisenman RN. The MYC transcription factor network: balancing metabolism, proliferation and oncogenesis. Front Med 2018;12:412–425.

4. Meyer N, Penn LZ. Reflecting on 25 years with MYC. Nat Rev Cancer 2008;8:976–990.

5. Stine ZE, Walton ZE, Altman BJ, Hsieh AL, Dang CV. MYC, metabolism, and cancer. Cancer Discov 2015; 5:1024–1039.

6. van Riggelen J, Yetil A, Felsher DW. MYC as a regulator of ribosome biogenesis and protein synthesis. Nat Rev Cancer 2010;10:301–309.

7. Wahlstrom T, Henriksson MA. Impact of MYC in regulation of tumor cell metabolism. Biochim Biophys Acta 2015;1849:563–569.

8. Carroll PA, Freie BW, Cheng PF, Kasinathan S, Gu H, Hedrich T, Dowdle JA, Venkataramani V, Ramani V, Wu X, Raftery D, Shendure J, Ayer DE, Muller CH, Eisenman RN. The glucose-sensing transcription factor MLX balances metabolism and stress to suppress apoptosis and maintain spermatogenesis. PLoS Biol 2021;19:e3001085.

9. Kuznetsov VA, Singh O, Jenjaroenpun P. Statistics of protein-DNA binding and the total number of binding sites for a transcription factor in the mammalian genome. BMC Genomics 2010;11(Suppl 1):S12.

10. Levens D. Cellular MYCro economics: balancing MYC function with MYC expression. Cold Spring Harb Perspect Med 2013;3:a014233.

11. Sabo A, Amati B. Genome recognition by MYC. Cold Spring Harb Perspect Med 2014;4:a014191.

12. Dang CV, O'Donnell KA, Zeller KI, Nguyen T, Osthus RC, Li F. The c-Myc target gene network. Semin Cancer Biol 2006;16:253–264.

13. Diolaiti D, McFerrin L, Carroll PA, Eisenman RN. Functional interactions among members of the MAX and MLX transcriptional network during oncogenesis. Biochim Biophys Acta 2015;1849:484–500.

14. Kalkat M, De Melo J, Hickman KA, Lourenco C, Redel C, Resetca D, Tamachi A, Tu WB, Penn LZ. MYC deregulation in primary human cancers. Genes (Basel) 2017; 8:151.

15. Liu J, Levens D. Making myc. Curr Top Microbiol Immunol 2006;302:1–32.

16. Tu WB, Shiah YJ, Lourenco C, Mullen PJ, Dingar D, Redel C, Tamachi A, Ba-Alawi W, Aman A, Al-Awar R, Cescon DW, Haibe-Kains B, Arrowsmith CH, Raught B, Boutros PC, Penn LZ. MYC interacts with the G9a histone methyltransferase to drive transcriptional repression and tumorigenesis. Cancer Cell 2018;34:579–595 e8.

17. Wilde BR, Ayer DE. Interactions between Myc and MondoA transcription factors in metabolism and tumourigenesis. Br J Cancer 2015;113:1529–1533.

18. Grandori C, Cowley SM, James LP, Eisenman RN. The Myc/Max/Mad network and the transcriptional control of cell behavior. Annu Rev Cell Dev Biol 2000;16:653–699.

19. McArthur GA, Laherty CD, Queva C, Hurlin PJ, Loo L, James L, Grandori C, Gallant P, Shiio Y, Hokanson WC, Bush AC, Cheng PF, Lawrence QA, Pulverer B, Koskinen PJ, Foley KP, Ayer DE, Eisenman RN. The Mad protein family links transcriptional repression to cell differentiation. Cold Spring Harb Symp Quant Biol 1998; 63:423–433.

20. Prochownik E, Wang H. Normal and neoplastic growth suppression by the extended Myc network. Cells 2022; 11:747.

21. Gartel AL, Shchors K. Mechanisms of c-myc-mediated transcriptional repression of growth arrest genes. Exp Cell Res 2003;283:17–21.

22. Herkert B, Eilers M. Transcriptional repression: the dark side of myc. Genes Cancer 2010;1:580–586.

23. Nesbit CE, Tersak JM, Prochownik EV. MYC oncogenes and human neoplastic disease. Oncogene 1999; 18:3004–3016.

24. Billin AN, Ayer DE. The Mlx network: evidence for a parallel Max-like transcriptional network that regulates energy metabolism. Curr Top Microbiol Immunol 2006; 302:255–278.

25. Wang H, Dolezal JM, Kulkarni S, Lu J, Mandel J, Jackson LE, Alencastro F, Duncan AW, Prochownik EV. Myc and ChREBP transcription factors cooperatively regulate normal and neoplastic hepatocyte proliferation in mice. J Biol Chem 2018;293:14740–14757.

26. Jeong YS, Kim D, Lee YS, Kim HJ, Han JY, Im SS, Chong HK, Kwon JK, Cho YH, Kim WK, Osborne TF, Horton JD, Jun HS, Ahn YH, Ahn SM, Cha JY. Integrated expression profiling and genome-wide analysis of ChREBP targets reveals the dual role for ChREBP in glucose-regulated gene expression. PLoS One 2011;6: e22544.

27. Poungvarin N, Chang B, Imamura M, Chen J, Moolsuwan K, Sae-Lee C, Li W, Chan L. Genome-wide analysis of ChREBP binding sites on male mouse liver and white adipose chromatin. Endocrinology 2015; 156:1982–1994.

28. Collier JJ, Zhang P, Pedersen KB, Burke SJ, Haycock JW, Scott DK. c-Myc and ChREBP regulate glucose-mediated expression of the L-type pyruvate kinase gene in INS-1-derived 832/13 cells. Am J Physiol Endocrinol Metab 2007;293:E48–E56.

29. Zhang P, Metukuri MR, Bindom SM, Prochownik EV, O'Doherty RM, Scott DK. c-Myc is required for the CHREBP-dependent activation of glucose-responsive genes. Mol Endocrinol 2010;24:1274–1286.

30. Billin AN, Eilers AL, Queva C, Ayer DE. Mlx, a novel Max-like BHLHZip protein that interacts with the Max network of transcription factors. J Biol Chem 1999; 274:36344–36350.

31. Billin AN, Eilers AL, Coulter KL, Logan JS, Ayer DE. MondoA, a novel basic helix-loop-helix-leucine zipper transcriptional activator that constitutes a positive branch of a max-like network. Mol Cell Biol 2000; 20:8845–8854.

32. Hurlin PJ, Queva C, Eisenman RN. Mnt: a novel Max-interacting protein and Myc antagonist. Curr Top Microbiol Immunol 1997;224:115–121.

33. Schaub FX, Dhankani V, Berger AC, Trivedi M, Richardson AB, Shaw R, Zhao W, Zhang X, Ventura A, Liu Y, Ayer DE, Hurlin PJ, Cherniack AD, Eisenman RN, Bernard B, Grandori C; Cancer Genome Atlas Network. Pan-cancer alterations of the MYC oncogene and its proximal network across the Cancer Genome Atlas. Cell Syst 2018;6:282–300 e2.

34. Chinsky JM, Singh R, Ficicioglu C, van Karnebeek CDM, Grompe M, Mitchell G, Waisbren SE, Gucsavas-Calikoglu M, Wasserstein MP, Coakley K, Scott CR. Diagnosis and treatment of tyrosinemia type I: a US and Canadian consensus group review and recommendations. Genet Med 2017;19.

35. Grompe M, Lindstedt S, al-Dhalimy M, Kennaway NG, Papaconstantinou J, Torres-Ramos CA, Ou CN, Finegold M. Pharmacological correction of neonatal lethal hepatic dysfunction in a murine model of hereditary tyrosinaemia type I. Nat Genet 1995;10:453–460.

36. Russo PA, Mitchell GA, Tanguay RM. Tyrosinemia: a review. Pediatr Dev Pathol 2001;4:212–221.

37. Edmunds LR, Otero PA, Sharma L, D'Souza S, Dolezal JM, David S, Lu J, Lamm L, Basantani M, Zhang P, Sipula IJ, Li L, Zeng X, Ding Y, Ding F, Beck ME, Vockley J, Monga SP, Kershaw EE, O'Doherty RM, Kratz LE, Yates NA, Goetzman EP, Scott D, Duncan AW, Prochownik EV. Abnormal lipid processing but normal long-term repopulation potential of myc-/- hepatocytes. Oncotarget 2016; 7:30379–30395.

38. Michalopoulos GK. Liver regeneration after partial hepatectomy: critical analysis of mechanistic dilemmas. Am J Pathol 2010;176:2–13.

39. Dubois NC, Adolphe C, Ehninger A, Wang RA, Robertson EJ, Trumpp A. Placental rescue reveals a sole requirement for c-Myc in embryonic erythroblast survival and hematopoietic stem cell function. Development 2008;135:2455–2465.

40. Graves JA, Wang Y, Sims-Lucas S, Cherok E, Rothermund K, Branca MF, Elster J, Beer-Stolz D, Van Houten B, Vockley J, Prochownik EV. Mitochondrial structure, function and dynamics are temporally controlled by c-Myc. PLoS One 2012;7:e37699.

41. Landay M, Oster SK, Khosravi F, Grove LE, Yin X, Sedivy J, Penn LZ, Prochownik EV. Promotion of growth and apoptosis in c-myc nullizygous fibroblasts by other members of the myc oncoprotein family. Cell Death Differ 2000;7:697–705.

42. Trumpp A, Refaeli Y, Oskarsson T, Gasser S, Murphy M, Martin GR, Bishop JM. c-Myc regulates mammalian body size by controlling cell number but not cell size. Nature 2001;414:768–773.

43. Wang H, Mannava S, Grachtchouk V, Zhuang D, Soengas MS, Gudkov AV, Prochownik EV, Nikiforov MA. c-Myc depletion inhibits proliferation of human tumor cells at various stages of the cell cycle. Oncogene 2008; 27:1905–1915.

44. Donato M, Hamidian Jahromi A, Andrade AI, Kim R, Chaudhery SI, Sangster G. Hepatic adenomatosis: a rare but important liver disease with severe clinical implications. Int Surg 2015;100:903–907.

45. Qu A, Jiang C, Cai Y, Kim JH, Tanaka N, Ward JM, Shah YM, Gonzalez FJ. Role of Myc in hepatocellular proliferation and hepatocarcinogenesis. J Hepatol 2014; 60:331–338.

46. Jackson LE, Kulkarni S, Wang H, Lu J, Dolezal JM, Bharathi SS, Ranganathan S, Patel MS, Deshpande R, Alencastro F, Wendell SG, Goetzman ES, Duncan AW, Prochownik EV. Genetic dissociation of glycolysis and the TCA cycle affects neither normal nor neoplastic proliferation. Cancer Res 2017;77:5795–5807.

47. Wang H, Lu J, Mandel JA, Zhang W, Schwalbe M, Gorka J, Liu Y, Marburger B, Wang J, Ranganathan S, Prochownik EV. Patient-derived mutant forms of NFE2L2/NRF2 drive aggressive murine hepatoblastomas. Cell Mol Gastroenterol Hepatol 2021; 12:199–228.

48. Subramanian A, Tamayo P, Mootha VK, Mukherjee S, Ebert BL, Gillette MA, Paulovich A, Pomeroy SL, Golub TR, Lander ES, Mesirov JP. Gene set enrichment analysis: a knowledge-based approach for interpreting genome-wide expression profiles. Proc Natl Acad Sci U S A 2005;102:15545–15550.

49. Mounir M, Lucchetta M, Silva TC, Olsen C, Bontempi G, Chen X, Noushmehr H, Colaprico A, Papaleo E. New functionalities in the TCGAbiolinks package for the study and integration of cancer data from GDC and GTEx. PLoS Comput Biol 2019;15:e1006701.

50. Gu Z, Eils R, Schlesner M. Complex heatmaps reveal patterns and correlations in multidimensional genomic data. Bioinformatics 2016;32:2847–2849.

51. Dolezal JM, Wang H, Kulkarni S, Jackson L, Lu J, Ranganathan S, Goetzman ES, Bharathi SS, Beezhold K, Byersdorfer CA, Prochownik EV. Sequential adaptive changes in a c-Myc-driven model of hepatocellular carcinoma. J Biol Chem 2017;292:10068–10086.

52. Havula E, Hietakangas V. Sugar sensing by ChREBP/Mondo-Mlx-new insight into downstream regulatory networks and integration of nutrient-derived signals. Curr Opin Cell Biol 2018;51:89–96.

53. Hsieh AL, Walton ZE, Altman BJ, Stine ZE, Dang CV. MYC and metabolism on the path to cancer. Semin Cell Dev Biol 2015;43:11–21.

54. Li F, Wang Y, Zeller KI, Potter JJ, Wonsey DR, O'Donnell KA, Kim JW, Yustein JT, Lee LA, Dang CV. Myc stimulates nuclearly encoded mitochondrial genes and mitochondrial biogenesis. Mol Cell Biol 2005; 25:6225–6234.

55. ENCODE Project Consortium, Moore JE, Purcaro MJ, Pratt HE, Epstein CB, Shoresh N, Adrian J, Kawli T, Davis CA, Dobin A, Kaul R, Halow J, Van Nostrand EL, Freese P, Gorkin DU, Shen Y, He Y, Mackiewicz M, Pauli-Behn F, Williams BA, Mortazavi A, Keller CA, Zhang XO, Elhajjajy SI, Huey J, Dickel DE, Snetkova V, Wei X, Wang X, Rivera-Mulia JC, Rozowsky J, Zhang J, Chhetri SB, Zhang J, Victorsen A, White KP, Visel A, Yeo GW, Burge CB, Lecuyer E, Gilbert DM, Dekker J, Rinn J, Mendenhall EM, Ecker JR, Kellis M, Klein RJ, Noble WS, Kundaje A, Guigo R, Farnham PJ, Cherry JM, Myers RM, Ren B, Graveley BR, Gerstein MB, Pennacchio LA, Snyder MP, Bernstein BE, Wold B, Hardison RC, Gingeras TR, Stamatoyannopoulos JA, Weng Z. Expanded encyclopaedias of DNA elements in the human and mouse genomes. Nature 2020; 583:699–710.

56. Kulakovskiy IV, Vorontsov IE, Yevshin IS, Sharipov RN, Fedorova AD, Rumynskiy EI, Medvedeva YA, Magana-

Mora A, Bajic VB, Papatsenko DA, Kolpakov FA, Makeev VJ. HOCOMOCO: towards a complete collection of transcription factor binding models for human and mouse via large-scale ChIP-Seq analysis. Nucleic Acids Res 2018;46:D252–D259.

57. Wang H, Lu J, Edmunds LR, Kulkarni S, Dolezal J, Tao J, Ranganathan S, Jackson L, Fromherz M, Beer-Stolz D, Uppala R, Bharathi S, Monga SP, Goetzman ES, Prochownik EV. Coordinated activities of multiple Myc-dependent and Myc-independent biosynthetic pathways in hepatoblastoma. J Biol Chem 2016; 291:26241–26251.

58. Cotter D, Guda P, Fahy E, Subramaniam S. MitoProteome: mitochondrial protein sequence database and annotation system. Nucleic Acids Res 2004; 32:D463–D467.

59. Mandel J, Wang H, Normolle DP, Chen W, Yan Q, Lucas PC, Benos PV, Prochownik EV. Expression patterns of small numbers of transcripts from functionally-related pathways predict survival in multiple cancers. BMC Cancer 2019;19:686.

60. Karim S, Adams DH, Lalor PF. Hepatic expression and cellular distribution of the glucose transporter family. World J Gastroenterol 2012;18:6771–6781.

61. Kim JW, Dang CV. Cancer's molecular sweet tooth and the Warburg effect. Cancer Res 2006;66:8927–8930.

62. Miller DM, Thomas SD, Islam A, Muench D, Sedoris K. c-Myc and cancer metabolism. Clin Cancer Res 2012; 18:5546–5553.

63. Osthus RC, Shim H, Kim S, Li Q, Reddy R, Mukherjee M, Xu Y, Wonsey D, Lee LA, Dang CV. Deregulation of glucose transporter 1 and glycolytic gene expression by c-Myc. J Biol Chem 2000;275:21797–21800.

64. Thorens B. GLUT2, glucose sensing and glucose homeostasis. Diabetologia 2015;58:221–232.

65. Ward PS, Thompson CB. Metabolic reprogramming: a cancer hallmark even Warburg did not anticipate. Cancer Cell 2012;21:297–308.

66. Chadt A, Al-Hasani H. Glucose transporters in adipose tissue, liver, and skeletal muscle in metabolic health and disease. Pflugers Arch 2020;472:1273–1298.

67. Muller I, Larsson K, Frenzel A, Oliynyk G, Zirath H, Prochownik EV, Westwood NJ, Henriksson MA. Targeting of the MYCN protein with small molecule c-MYC inhibitors. PLoS One 2014;9:e97285.

68. Soucek L, Evan GI. The ups and downs of Myc biology. Curr Opin Genet Dev 2010;20:91–95.

69. Goetzman ES, Prochownik EV. The role for Myc in coordinating glycolysis, oxidative phosphorylation, glutaminolysis, and fatty acid metabolism in normal and neoplastic tissues. Front Endocrinol (Lausanne) 2018; 9:129.

70. Greco D, Kotronen A, Westerbacka J, Puig O, Arkkila P, Kiviluoto T, Laitinen S, Kolak M, Fisher RM, Hamsten A, Auvinen P, Yki-Jarvinen H. Gene expression in human NAFLD. Am J Physiol Gastrointest Liver Physiol 2008; 294:G1281–G1287.

71. Pello OM, De Pizzol M, Mirolo M, Soucek L, Zammataro L, Amabile A, Doni A, Nebuloni M, Swigart LB, Evan GI, Mantovani A, Locati M. Role of c-MYC in alternative activation of human macrophages and tumor-associated macrophage biology. Blood 2012; 119:411–421.

72. Torbenson M. Hepatic adenomas: classification, controversies, and consensus. Surg Pathol Clin 2018; 11:351–366.

73. Zhang W, Meyfeldt J, Wang H, Kulkarni S, Lu J, Mandel JA, Marburger B, Liu Y, Gorka JE, Ranganathan S, Prochownik EV. beta-Catenin mutations as determinants of hepatoblastoma phenotypes in mice. J Biol Chem 2019;294:17524–17542.

74. Sylvester KG, Colnot S. Hippo/YAP, beta-catenin, and the cancer cell: a "menage a trois" in hepatoblastoma. Gastroenterology 2014;147:562–565.

75. Prochownik EV. Reconciling the biological and transcriptional variability of hepatoblastoma with its mutational uniformity. Cancers (Basel) 2021;13:1996.

76. Itoh T, Miyajima A. Liver regeneration by stem/progenitor cells. Hepatology 2014;59:1617–1626.

77. Miyaoka Y, Ebato K, Kato H, Arakawa S, Shimizu S, Miyajima A. Hypertrophy and unconventional cell division of hepatocytes underlie liver regeneration. Curr Biol 2012;22:1166–1175.

78. Hofmann JW, Zhao X, De Cecco M, Peterson AL, Pagliaroli L, Manivannan J, Hubbard GB, Ikeno Y, Zhang Y, Feng B, Li X, Serre T, Qi W, Van Remmen H, Miller RA, Bath KG, de Cabo R, Xu H, Neretti N, Sedivy JM. Reduced expression of MYC increases longevity and enhances healthspan. Cell 2015; 160:477–488.

79. Camarda R, Williams J, Goga A. In vivo Reprogramming of cancer metabolism by MYC. Front Cell Dev Biol 2017; 5:35.

80. Wang H, Lu J, Kulkarni S, Zhang W, Gorka JE, Mandel JA, Goetzman ES, Prochownik EV. Metabolic and oncogenic adaptations to pyruvate dehydrogenase inactivation in fibroblasts. J Biol Chem 2019; 294:5466–5486.

81. Mathsyaraja H, Freie B, Cheng PF, Babaeva E, Catchpole JT, Janssens D, Henikoff S, Eisenman RN. Max deletion destabilizes MYC protein and abrogates Emicro-Myc lymphomagenesis. Genes Dev 2019; 33:1252–1264.

82. Prochownik EV, Wang H. The metabolic fates of pyruvate in normal and neoplastic cells. Cells 2021; 10:762.

83. Zirath H, Frenzel A, Oliynyk G, Segerstrom L, Westermark UK, Larsson K, Munksgaard Persson M, Hultenby K, Lehtio J, Einvik C, Pahlman S, Kogner P, Jakobsson PJ, Henriksson MA. MYC inhibition induces metabolic changes leading to accumulation of lipid droplets in tumor cells. Proc Natl Acad Sci U S A 2013; 110:10258–10263.

84. Wang H, Sharma L, Lu J, Finch P, Fletcher S, Prochownik EV. Structurally diverse c-Myc inhibitors share a common mechanism of action involving ATP depletion. Oncotarget 2015;6:15857–15870.

85. Michelotti GA, Machado MV, Diehl AM. NAFLD, NASH and liver cancer. Nat Rev Gastroenterol Hepatol 2013; 10:656–665.

86. Ioannou GN. Epidemiology and risk-stratification of NAFLD-associated HCC. J Hepatol 2021;75:1476–1484.

87. Bluteau O, Jeannot E, Bioulac-Sage P, Marques JM, Blanc JF, Bui H, Beaudoin JC, Franco D, Balabaud C, Laurent-Puig P, Zucman-Rossi J. Bi-allelic inactivation of TCF1 in hepatic adenomas. Nat Genet 2002;32:312–315.

88. Lee S, Karas PJ, Hadley CC, Bayley VJ, Khan AB, Jalali A, Sweeney AD, Klisch TJ, Patel AJ. The role of Merlin/NF2 loss in meningioma biology. Cancers (Basel) 2019;11:1633.

89. Navarro A, Yin P, Monsivais D, Lin SM, Du P, Wei JJ, Bulun SE. Genome-wide DNA methylation indicates silencing of tumor suppressor genes in uterine leiomyoma. PLoS One 2012;7:e33284.

90. Williams EA, Wakimoto H, Shankar GM, Barker FG 2nd, Brastianos PK, Santagata S, Sokol ES, Pavlick DC, Shah N, Reddy A, Venstrom JM, Alexander BM, Ross JS, Cahill DP, Ramkissoon SH, Juratli TA. Frequent inactivating mutations of the PBAF complex gene PBRM1 in meningioma with papillary features. Acta Neuropathol 2020;140:89–93.

91. Marengo A, Rosso C, Bugianesi E. Liver cancer: connections with obesity, fatty liver, and cirrhosis. Annu Rev Med 2016;67:103–117.

92. Brunt EM, Wong VW, Nobili V, Day CP, Sookoian S, Maher JJ, Bugianesi E, Sirlin CB, Neuschwander-Tetri BA, Rinella ME. Nonalcoholic fatty liver disease. Nat Rev Dis Primers 2015;1:15080.

93. Wang H, Lu J, Dolezal J, Kulkarni S, Zhang W, Chen A, Gorka J, Mandel JA, Prochownik EV. Inhibition of hepatocellular carcinoma by metabolic normalization. PLoS One 2019;14:e0218186.

94. Baena E, Gandarillas A, Vallespinos M, Zanet J, Bachs O, Redondo C, Fabregat I, Martinez AC, de Alboran IM. c-Myc regulates cell size and ploidy but is not essential for postnatal proliferation in liver. Proc Natl Acad Sci U S A 2005;102:7286–7291.

95. de Alboran IM, O'Hagan RC, Gartner F, Malynn B, Davidson L, Rickert R, Rajewsky K, DePinho RA, Alt FW. Analysis of C-MYC function in normal cells via conditional gene-targeted mutation. Immunity 2001;14:45–55.

96. Ventura A, Kirsch DG, McLaughlin ME, Tuveson DA, Grimm J, Lintault L, Newman J, Reczek EE, Weissleder R, Jacks T. Restoration of p53 function leads to tumour regression in vivo. Nature 2007;445:661–665.

97. Folch J, Lees M, Sloane Stanley GH. A simple method for the isolation and purification of total lipides from animal tissues. J Biol Chem 1957;226:497–509.

98. Jouihan H. Measurement of liver triglyceride content. Bioprotocol 2012;2:e223.

99. Zhu LJ, Gazin C, Lawson ND, Pages H, Lin SM, Lapointe DS, Green MR. ChIPpeakAnno: a Bioconductor package to annotate ChIP-seq and ChIP-chip data. BMC Bioinformatics 2010;11:237.

100. The ENCODE Project Consortium. An integrated encyclopedia of DNA elements in the human genome. Nature 2012;489:57–74.

Correspondence
Address correspondence to: Edward V. Prochownik, MD, PhD, Division of Hematology/Oncology, Children's Hospital of Pittsburgh, Rangos Research Center, Room 5124, 4401 Penn Avenue, Pittsburgh, Pennsylvania 15224. e-mail: procev@chp.edu; fax: (412) 692-5228.

CRediT Authorship Contributions

Huabo Wang, PhD (Conceptualization: Lead; Data curation: Lead; Formal analysis: Lead; Investigation: Lead; Writing – original draft: Equal; Writing – review & editing: Equal)

Jie Lu (Investigation: Equal)

Frances Alencastro (Investigation: Equal)

Alexander Roberts (Investigation: Supporting)

Julia Fiedor (Investigation: Supporting)

Patrick Carroll (Resources: Supporting)

Robert N. Eisenman (Resources: Supporting)

Sarangarajan Ranganathan (Formal analysis: Supporting)

Michael Torbenson (Formal analysis: Equal)

Andrew W. Duncan (Conceptualization: Equal; Funding acquisition: Equal; Investigation: Equal; Supervision: Equal)

Edward V. Prochownik (Conceptualization: Lead; Data curation: Equal; Formal analysis: Lead; Funding acquisition: Lead; Investigation: Lead; Supervision: Lead; Writing – original draft: Lead; Writing – review & editing: Lead)